ACS OMEGA

Open Access

http://pubs.acs.org/journal/acsodf

Article

Synthesis, Characterization, In Silico DFT, Molecular Docking, and Dynamics Simulation Studies of Phenylhydrazono Phenoxyquinolones for Their Hypoglycemic Efficacy

Narayanaswamy Lohitha, Peruru Hemanth Kumar, Sundaramoorthy Sarveswari, Sanket Rathod, Somdatta Chaudhari, Yasinalli Tamboli, Imadul Islam,* and Vijayaparthasarathi Vijayakumar*

Cite This: *ACS Omega* 2024, 9, 16384−16399

Read Online

ACCESS | Metrics & More | Article Recommendations | Supporting Information

ABSTRACT: A series of novel 24 phenylhydrazono phenoxyquinoline derivatives were synthesized with moderate to excellent yield and screened for their efficacy against the α-amylase enzyme through in silico studies. The structures were characterized using spectroscopic techniques such as ^{1}HNMR, ^{13}CNMR, and HREI-MS. Comprehensive computational studies including, drug-likeness and ADMET profiling, quantum chemical calculations, molecular docking, and molecular dynamics (MD) simulation studies, were performed. A density functional theory study of the synthesized compounds indicated a favorable reactivity profile. The synthesized novel analogues were docked against α-amylase (PDB 6OCN) enzymes to investigate the binding interactions. Based on the docking studies, one of the compounds was found to be the hit with the highest negative binding affinity for α-amylase. A MD simulation study indicated stable binding throughout the simulation.

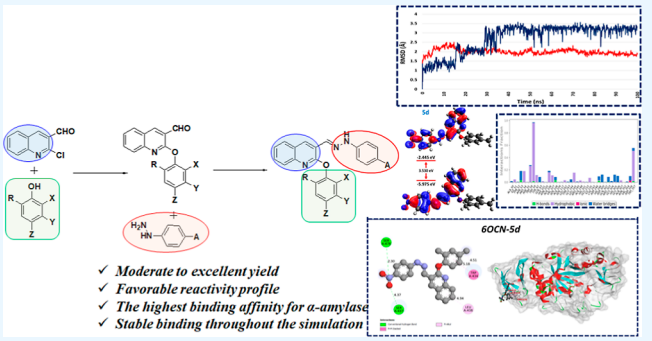

INTRODUCTION

Heterocyclic compound precursors find broad application in biological and pharmaceutical contexts. Among these, nitrogen-containing compounds stand out as being particularly prominent in drug discovery research. Medicinal chemists design and develop novel building blocks of heterocyclic motifs that exhibit prominent biological responses to the targeted reactive species or diseases.[1] 2-Chloroquinoline scaffolds are interesting precursors because of their range of biological activities,[2] and these compounds have attracted the attention of many scientific research fields such as material science, optics, agriculture, medicinal chemistry, and other developing areas.[3] One of the quinoline derivatives is used as an antiasthma agent.[4]

Over the past few decades, many researchers have focused on synthetic heterocyclic compounds, which have many biological and medicinal applications.[5,6] Quinoline-core containing molecules exhibit numerous biological and pharmaceutical activities such as antifungal,[7] antimalarial,[8] anticancer,[9] anti-HIV,[10] free radical scavenging,[11] antihypertensive,[12] and antituberculosis.[13] Moreover, some fluorinated and nonfluorinated quinoline derivatives are used as antibiotics and antimicrobial drugs (Figure 1), such as nadifloxacin (an antibiotic used for the treatment of staphylococcal infection),[14] ciprofloxacin, and grepafloxacin (an antibacterial agent).[15]

Antioxidants are key in diabetes as low levels of antioxidants can lead to complications. Plasma antioxidants in the blood have been linked to the development of diabetes mellitus (DM), and regulating the levels of radical scavengers is impaired as the disease progresses.[16] An increasing level of glucose in the blood is referred to as hyperglycemia; this occurs as a result of the aberrant function of insulin. Any destruction of the cells causes insulin secretion to be restricted or reduced, resulting in uncontrolled blood glucose levels.[17] DM consequences have been linked to oxidative stress, including retinopathy and atherosclerotic vascular disease, which is the leading cause of mortality in diabetic patients. There are various pathways through which DM can be inhibited, one of which is via enzyme inhibition methods.[18] According to previous reports, hyperglycemia can cause the nonenzymatic glycosylation of numerous proteins, which can lead to chronic diabetic problems. As a result, controlling postprandial blood glucose is crucial for diabetes therapy and preventing chronic vascular problems.[19] By partially inhibiting the enzyme reaction of complex carbohydrates, α-amylase inhibitors may contribute by preventing postprandial hyperglycemia and,

Received: January 3, 2024
Revised: March 9, 2024
Accepted: March 19, 2024
Published: March 28, 2024

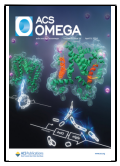

Scheme 1. Synthesis of Phenylhydrazono Phenoxyquinolines (5a−5x)

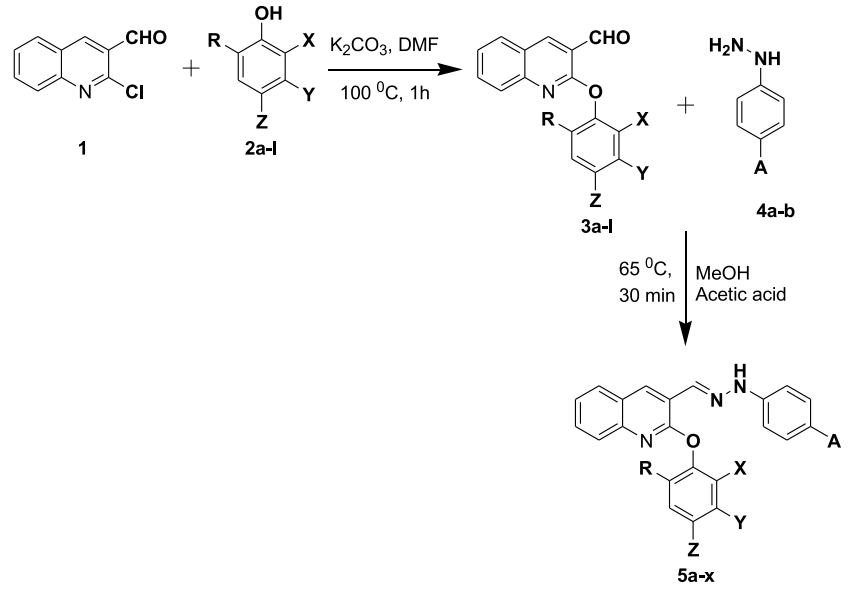

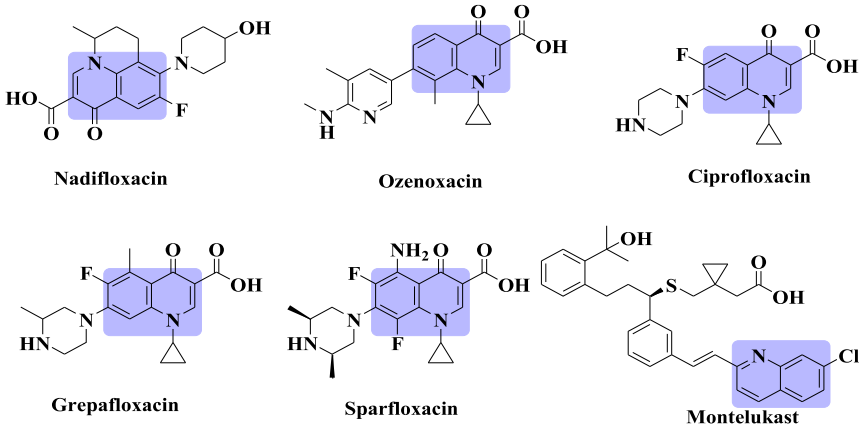

Figure 1. Fused quinolines are antiasthma, antibiotic, and antimicrobial drugs.

hence, delaying glucose absorption.[20] In patients with type 2 diabetes, acarbose, voglibose, and miglitol are commonly used either alone or in combination with insulin secretagogues. α-Amylase inhibitors have been used as targets for drug development in the treatment of diabetes, obesity, and hyperlipidemia. The development of efficient nitrogen-based α-amylase inhibitors with excellent specificity and efficacy could improve DM treatment. The objective of this research was to design novel phenylhydrazono phenoxyquinoline derivatives and synthesize, characterize, and validate them through in silico studies as suitable α-amylase inhibitors for DM treatment. The development of efficient nitrogen-based α-amylase inhibitors with excellent specificity and efficacy has the potential to improve the DM treatment.

The results of the present current in silico studies showed that the newly synthesized **5a−5x** compounds had antidiabetic activity by good binding activity of α-amylase and α-glucosidase enzymes, and these compounds were the best binding targets.

RESULTS AND DISCUSSION

Chemistry. The synthesis of phenylhydrazono phenoxyquinolines (**5a−5x**) is demonstrated in Scheme 1. Initially, the core nucleus 2-chloroquinoline was treated with various substituted phenolic compounds (**2a−i**) in the presence of K_2CO_3 in DMF at 100 °C for 1 h, which affords the desired substituted 2-phenoxyquinoline-3-carbaldehyde (**3a−3i**).[21] Subsequently, hydrazide Schiff's bases [3-((2-(4-nitro/bromophenyl)hydrazono)methyl)-2-phenoxyquinolines (**5a−5x**)] were synthesized by a catalytic amount of acetic acid using appropriate aldehyde (**3a−3i**) with substituted (4-bromo or nitro) phenyl hydrazine (**4a−4b**) in methanol at 65 °C for 30 min. The ^{1}H nuclear magnetic resonance (NMR) spectrum of compound 3-((2-(4-nitrophenyl)hydrazono)methyl)-2-phenoxyquinoline (**5a**) exhibited chemical shifts in the aromatic region ranging from δ 11.63 to 7.32−7.27 ppm. The singlet at δ 11.63 ppm is assigned to the proton singlet of the amino function group, and δ 8.95 ppm is for the imine proton singlet. The ^{13}C NMR spectrum exhibited the aryl carbons of phenylhydrazono phenoxyquinoline signals ranging from δ 153.82 to 112.11 ppm, the extreme downfield signal at δ 159.00 ppm assigned to the phenoxy carbon at C-2. All of these spectral data confirmed the formation of the desired molecule, further supported by the observation of m/z at 384.1222 in the mass spectrum [HRMS-ESI (m/z)] for $C_{22}H_{16}N_4O_3$ $[M]^+$ = 384.1222. The chemical shift values of

https://doi.org/10.1021/acsomega.4c00079
ACS Omega 2024, 9, 16384−16399

Table 1. Predicted Physicochemical and Drug-Likeness Properties of the Synthesized Phenylhydrazono Phenoxyquinoline Derivatives (5a−5x)[a]

compound	MW (g/mol)	*m* log *P*	HBA	HBD	MR	TPSA	nRot	Lipinski's rule (Ro5)	Veber's rule
5a	384.39	3.84	5	1	114.56	92.33	6	+	+
5b	398.41	3.24	5	1	119.52	92.33	6	+	+
5c	398.41	3.24	5	1	119.52	92.33	6	+	+
5d	412.44	3.45	5	1	124.49	92.33	6	+	+
5e	418.83	4.32	5	1	119.57	92.33	6	+	+
5f	418.83	4.32	5	1	119.57	92.33	6	+	+
5g	418.83	4.32	5	1	119.57	92.33	6	+	+
5h	453.28	4.8	5	1	124.58	92.33	6	+	+
5i	463.28	4.43	5	1	122.26	92.33	6	+	+
5j	440.49	3.86	5	1	133.83	92.33	7	+	+
5k	398.41	3.24	5	1	119.52	92.33	6	+	+
5L	444.44	2.42	7	1	127.54	110.79	8	+	+
5m	418.29	4.57	3	1	113.44	46.51	5	+	+
5n	432.31	4.78	3	1	118.4	46.51	5	+	+
5o	432.31	4.78	3	1	118.4	46.51	5	+	+
5p	446.34	4.99	3	1	123.37	46.51	5	+	+
5q	452.73	5.05	3	1	118.45	46.51	5	+	+
5r	452.73	5.05	3	1	118.45	46.51	5	+	+
5s	452.73	5.05	3	1	118.45	46.51	5	+	+
5t	487.18	5.52	3	1	123.46	46.51	5	+	+
5u	497.18	5.15	3	1	121.14	46.51	5	+	+
5v	474.39	5.39	3	1	132.71	46.51	6	+	+
5w	432.31	4.78	3	1	118.4	46.51	5	+	+
5x	478.34	3.88	5	1	126.42	64.97	7	+	+

[a]+passed; −failed.

the remaining compounds of the series were also assigned similarly and are included in the Experimental Section.

Computational Studies. *Drug-Likeness and In Silico ADMET Prediction.* The drug-likeness of synthesized phenylhydrazono phenoxyquinoline derivatives (**5a−5x**) was assessed by evaluating a set of physicochemical properties aligned with established rules. This analysis incorporated Lipinski's rule of five and Veber's rule to estimate the drug-likeness attributes. Key parameters such as molecular weight, lipophilicity, hydrogen bond donors and acceptors, molecular refractivity, topological polar surface area, and number of rotatable bonds were scrutinized to ascertain the drug-likeness and ADMET profile of synthesized compounds are detailed in Table 1. The findings from this investigation notably revealed that all of the synthesized compounds met the criteria set by these rules. The emphasis on drug-likeness aided in the initial categorization of compounds based on their inherent drug-like properties. This assessment is crucial in the early stages of drug discovery. The successful adherence to the drug-likeness criteria underscored the promise of these compounds for future drug development activities.

To assess the pharmacokinetic properties of the synthesized compounds (**5a−5x**), an in silico profiling was conducted using the pkCSM server. The results of the assessment are detailed in Table 2, showed promising characteristics across the various parameters. Notably, all of the compounds displayed high rates of intestinal absorption. Compound **5l** exhibited exceptional absorption at 100%. However, when examining their distribution, three key parameters were considered: the volume of distribution, blood−brain barrier (BBB) permeability, and central nervous system (CNS) permeability. The findings indicated a satisfactory volume of distribution for the compounds, suggesting a potentially favorable distribution of these compounds within the body. However, the compounds demonstrated poor permeability across both the BBB and CNS, indicating that they have a limited ability to pass into critical areas of the CNS. Moreover, the compounds were evaluated for their metabolic activity against key cytochrome P450 enzymes (CYPs). The results showed that all compounds were inactive against CYP2D6 but exhibited activity against CYP3A4, CYP1A2, CYP2C19, and CYP3A4. These findings indicate that the synthesized compounds possess significant metabolic activity in the human body.

The observed activity against various CYP enzymes suggested the potential for efficient metabolism and contributed positively to the pharmacological profiles of these enzymes. Despite promising pharmacokinetic attributes, the in silico toxicity assessment revealed interesting findings for the synthesized compounds. Except for compounds **5L**, **5o**, **5w**, and **5x**, all of the other compounds displayed AMES toxicity. This indicated the potential mutagenic properties of these compounds. However, synthesized compounds are hepatotoxic and might have adverse effects on liver cells. As these compounds demonstrate favorable pharmacokinetic profiles, the observed toxicities are significant concerns. Addressing these issues through structural modifications could enhance the safety of these compounds. Overall, these findings emphasize the importance of balancing efficacy with safety and highlight the need for further optimization of these compounds to achieve decreased toxicity.

Density Functional Theory Calculations. The synthesized phenylhydrazono phenoxyquinoline derivatives (**5a−5x**) were subjected to density functional theory (DFT) calculations. ORCA 4.2.1 at the B3LYP/def2-SVP level theory was used to carry out all of the calculations. The current study focused

https://doi.org/10.1021/acsomega.4c00079
ACS Omega 2024, 9, 16384−16399

Table 2. Predicted Pharmacokinetic (ADMET) Properties of the Synthesized Phenylhydrazono Phenoxyquinoline Derivatives (5a−5x)

compound	absorption	distribution			metabolism							excretion	toxicity	
	intestinal absorption (human)	VDs (human)	BBB permeability	CNS permeability	substrate		inhibitors					total clearance	AMES toxicity	hepatotoxicity
							CYP							
					2D6	3A4	1A2	2C19	2C9	2D6	3A4			
	numeric (% absorbed)	numeric (log L kg^{-1})	numeric (log BB)	numeric (log PS)	categorical (yes/no)							numeric (log mL min^{-1} kg^{-1})	categorical (Yes/No)	
5a	91.67	−0.32	−0.69	−1.74	no	yes	yes	yes	yes	no	yes	0.38	yes	yes
5b	89.08	−0.45	−0.38	−1.68	no	yes	yes	yes	yes	no	yes	0.39	yes	yes
5c	89.57	−0.43	−0.37	−1.68	no	yes	yes	yes	yes	no	yes	0.36	yes	yes
5d	89.37	−0.38	−0.34	−1.60	no	yes	yes	yes	yes	no	yes	0.38	yes	yes
5e	87.62	−0.45	−0.55	−1.64	no	yes	yes	yes	yes	no	yes	0.37	yes	yes
5f	87.93	−0.41	−0.53	−1.65	no	yes	yes	yes	yes	no	yes	0.25	yes	yes
5g	88.11	−0.42	−0.54	−1.64	no	yes	yes	yes	yes	no	yes	0.18	yes	yes
5h	86.45	−0.38	−0.69	−1.52	no	yes	yes	yes	yes	no	yes	0.30	yes	yes
5i	88.04	−0.41	−0.55	−1.61	no	yes	yes	yes	yes	no	yes	0.16	yes	yes
5j	89.42	−0.73	−0.64	−1.39	no	yes	yes	yes	yes	no	no	0.31	yes	yes
5k	89.39	−0.42	−0.36	−1.69	no	yes	yes	yes	yes	no	yes	0.38	yes	yes
5L	100.00	−0.68	−0.79	−2.15	no	yes	no	yes	yes	no	yes	0.27	no	yes
5m	90.88	−0.08	0.47	−1.21	no	yes	yes	yes	yes	no	yes	0.15	yes	yes
5n	90.68	−0.03	0.48	−1.19	no	yes	yes	yes	yes	no	yes	0.11	yes	yes
5o	90.55	−0.02	0.32	−0.82	no	yes	yes	yes	yes	no	yes	0.08	no	yes
5p	90.48	0.03	0.50	−1.18	no	yes	yes	yes	yes	no	yes	0.05	yes	yes
5q	89.22	−0.02	0.47	−1.19	no	yes	yes	yes	yes	no	yes	0.21	yes	yes
5r	89.22	−0.02	0.47	−1.19	no	yes	yes	yes	yes	no	yes	0.08	yes	yes
5s	89.09	−0.02	0.31	−0.82	no	yes	yes	yes	yes	no	yes	0.10	yes	yes
5t	87.56	0.04	0.47	−1.18	no	yes	yes	yes	yes	no	yes	0.13	yes	yes
5u	89.16	0.00	0.47	−1.19	no	yes	yes	yes	yes	no	yes	−0.01	yes	yes
5v	88.63	−0.50	0.38	−0.93	no	yes	yes	yes	yes	no	no	0.03	yes	yes
5w	90.68	−0.03	0.48	−1.19	no	yes	yes	yes	yes	no	yes	0.04	no	yes
5x	90.45	−0.23	0.37	−1.82	no	yes	yes	yes	yes	no	yes	0.41	no	yes

https://doi.org/10.1021/acsomega.4c00079
ACS Omega 2024, 9, 16384−16399

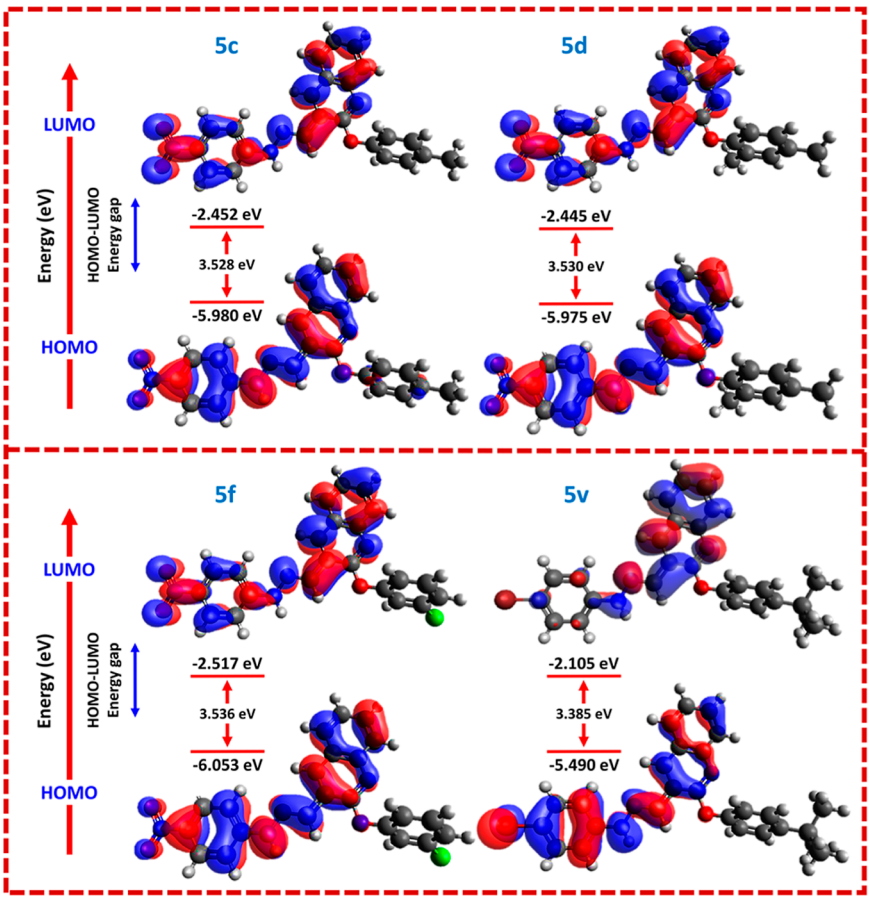

Figure 2. FMOs along with respective energies for the synthesized compounds have good binding affinity.

mainly on the estimation of various molecular properties and reactivity descriptors based on the energies of frontier molecular orbitals (FMOs).[22,23] The highest occupied molecular orbital (HOMO) energy, lowest unoccupied molecular orbital (LUMO) energy, and energy gap between the HOMO and LUMO were estimated to determine the reactivity of the compounds.[24] These values help in predicting the reactivity order among the synthesized compounds (**5a**−**5x**). The HOMO energy signifies the electron-donating ability of a molecule. On the other hand, the LUMO energy represents its electron-accepting capacity.[25,26] A smaller HOMO−LUMO gap generally suggests greater reactivity and greater potential for chemical interactions with biological molecular targets.[27,28] Figure 2 shows the FMOs of the compounds that exhibited a good binding affinity in the docking study. Other calculated chemical reactivity descriptors, such as dipole moment, ionization potential, electron affinity, electronegativity, chemical hardness, and electrophilicity, are detailed in Table 3. The chemical reactivity order based on the HOMO−LUMO energy gap from the highest to lowest reactivity among the synthesized phenylhydrazono phenoxyquinoline derivatives (**5a**−**5x**) is as follows: **5t** > **5u** > **5r** > **5s** > **5q** > **5x** > **5w** > **5v** > **5m** > **5o** > **5n** > **5p** > **5L** > **5c** > **5h** > **5d** > **5j** > **5k** > **5a** > **5b** > **5g** > **5f** > **5e**. Specifically, compound **5t** exhibited the smallest HOMO−LUMO energy gap, which indicates that it has the highest reactivity among the synthesized compounds. Moreover, compound **5u** displayed the highest dipole moment. This suggested a substantial separation of charges within the molecule, which might influence its interactions in various chemical environments. The calculated reactivity descriptors provided crucial insights into the behavior, electronic structure, and potential chemical interactions of synthesized compounds (**5a**−**5x**). The estimated ionization potential and electron affinity indicated a tendency to lose or gain electrons. However, their electronegativity and chemical hardness reflect their electron-attracting ability and stability. Electrophilicity helps to measure the propensity of a compound to undergo electrophilic reactions. These descriptors aided in elucidating the reactivity patterns of these compounds in various chemical processes. The results derived from these calculations will further help in identifying and prioritizing compounds based on their reactivity patterns.

Docking Study. The investigation focused on the molecular interactions and binding affinities of synthesized analogue **5a**−**5x** with α-amylase. A docking study was carried out to decipher the binding characteristics of the synthesized compounds. The results of the docking studies are presented in Table 4, which serves as a comprehensive repository of vital data on the binding interactions between these analogues and α-amylase. In this context, the synthesized analogue functioned as a ligand, while α-amylase served as the receptor. The in silico docking studies yielded insightful information about the binding energies of these designed molecules. Compound **5d** emerged as the most promising candidate because of its binding affinity of −9.2 kcal/mol for α-amylase. Further examination of the ligand−protein complex revealed fascinating aspects of the binding interaction. Conventional hydrogen bonds were formed between compound **5d** and specific amino acid residues within the α-amylase. Notably, SER478 and

https://doi.org/10.1021/acsomega.4c00079
ACS Omega 2024, 9, 16384−16399

Table 3. Calculated Energies of Chemical Reactivity Descriptors Based on the Energies of FMOs for Synthesized Phenylhydrazono Phenoxyquinoline Derivatives (5a−5x)[a]

<!—Col Count:11(code	HOMO (eV)	LUMO (eV)	HLG (eV)	DM (Debye)	IP (eV)	EA (eV)	χ (eV)	μ (eV)	η (eV)	ω (eV)
5a	−6.006	−2.474	3.532	6.376	6.006	2.474	4.240	−4.240	1.766	5.090
5b	−5.997	−2.465	3.532	6.382	5.997	2.465	4.231	−4.231	1.766	5.068
5c	−5.980	−2.452	3.528	6.851	5.980	2.452	4.216	−4.216	1.764	5.038
5d	−5.975	−2.445	3.530	6.805	5.975	2.445	4.210	−4.210	1.765	5.021
5e	−5.990	−2.451	3.539	7.414	5.990	2.451	4.221	−4.221	1.770	5.033
5f	−6.053	−2.517	3.536	5.598	6.053	2.517	4.285	−4.285	1.768	5.193
5g	−6.056	−2.523	3.533	4.973	6.056	2.523	4.290	−4.290	1.767	5.208
5h	−6.034	−2.505	3.529	5.862	6.034	2.505	4.270	−4.270	1.765	5.165
5i	−6.065	−2.533	3.532	4.826	6.065	2.533	4.299	−4.299	1.766	5.233
5j	−5.984	−2.454	3.530	6.903	5.984	2.454	4.219	−4.219	1.765	5.042
5k	−5.993	−2.462	3.531	6.604	5.993	2.462	4.228	−4.228	1.766	5.061
5L	−5.927	−2.403	3.524	7.744	5.927	2.403	4.165	−4.165	1.762	4.923
5m	−5.506	−2.119	3.387	2.008	5.506	2.119	3.813	−3.813	1.694	4.291
5n	−5.501	−2.104	3.397	2.019	5.501	2.104	3.803	−3.803	1.699	4.256
5o	−5.484	−2.093	3.391	2.441	5.484	2.093	3.789	−3.789	1.696	4.233
5p	−5.482	−2.078	3.404	2.454	5.482	2.078	3.780	−3.780	1.702	4.198
5q	−5.487	−2.112	3.375	3.015	5.487	2.112	3.800	−3.800	1.688	4.277
5r	−5.550	−2.182	3.368	1.461	5.550	2.182	3.866	−3.866	1.684	4.438
5s	−5.553	−2.183	3.370	0.683	5.553	2.183	3.868	−3.868	1.685	4.440
5t	−5.540	−2.178	3.362	1.476	5.540	2.178	3.859	−3.859	1.681	4.429
5u	−5.561	−2.195	3.366	0.577	5.561	2.195	3.878	−3.878	1.683	4.468
5v	−5.490	−2.105	3.385	2.359	5.490	2.105	3.798	−3.798	1.693	4.260
5w	−5.495	−2.112	3.383	2.235	5.495	2.112	3.804	−3.804	1.692	4.276
5x	−5.430	−2.051	3.379	4.010	5.430	2.051	3.741	−3.741	1.690	4.141

[a]DM: dipole moment in Debye; IP: ionization potential in eV; EA: electron affinity in eV; χ: electronegativity in eV; η: chemical hardness in eV; and ω: electrophilicity in eV.

SER437 were identified as pivotal contributors to this binding interaction. These hydrogen bonds, illustrated in Figure 3, underscored the specificity and precision of the binding between compound **5d** and α-amylase. Such interactions are of paramount importance as they are indicative of the stability and strength of the ligand−protein complex. These findings have significant implications for the potential therapeutic applications of these synthesized analogues. In particular, compound **5d** was found to be promising for diabetes management. The observed information in the docking study suggested that these analogues can effectively modulate the α-amylase activity. This attribute holds immense promise for glycemic control in individuals with DM. α-Amylase plays a pivotal role in carbohydrate digestion and glucose level regulation. Compound **5c** exhibited a substantial binding affinity of −9.1 kcal/mol, which reflected its potential as an effective ligand for α-amylase. Intriguingly, this compound engaged in conventional hydrogen bond formation with key amino acid residues within α-amylase, specifically GLN63 and HIS299, as shown in Figure 3. These hydrogen bonds are indicative of the precise nature of the molecular interaction. Similarly, compound **5f** demonstrated a commendable binding affinity of −9.1 kcal/mol. This reaffirmed its potential as a promising ligand. Notably, its interaction with α-amylase was characterized by the formation of a carbon−hydrogen bond with ALA198, as depicted in Figure 4. The identified interactions indicate the diverse binding mechanisms employed by these analogues with the targeted protein. The range of binding affinities was found between −7.7 and −9.2 kcal/mol. This highlights the structural diversity and versatility of the synthesized compounds with respect to α-amylase (PDB 6OCN). These findings collectively emphasize the potential of these synthesized analogues as valuable candidates for further investigation. The binding affinities and specific interactions identified in this study emphasize the capacity of these compounds to modulate α-amylase activity effectively. Such modulation holds significant promise for regulating carbohydrate digestion. Consequently, glycemic control in individuals with DM might also be possible. Furthermore, the diversity in binding mechanisms and affinities among these derivatives opens up possibilities for the development of promising α-amylase inhibitors. This study not only augments the understanding of ligand−protein interactions but also provides a foundation for the rational design and optimization of novel antidiabetics.

Molecular Dynamics Simulation. A molecular dynamics (MD) simulation study of compound **5d** against α-amylase (PDB 6OCN) was performed for 100 ns using Desmond software. The MD simulation study focused on identifying the binding stability and interactions throughout 100 ns. Compound **5d** showed the highest negative binding affinity and was found to be a hit against α-amylase (PDB 6OCN) in a docking study. MD simulation helped to assess the stability of the Cα structures from α-amylase (PDB 6OCN) with a bounded ligand structure over 100 ns. Statistical analysis of the rmsd, RMSF, protein−ligand contact, and interaction profile data was performed using the obtained MD trajectory. The rmsd was estimated for Cα (6OCN) and the bound hit (**5d**) from the protein−ligand complex. The rmsd plots of each sample were overlaid and are presented in Figure 5 to indicate the deviations in the rmsd values of Cα (6OCN) and **5d** present in over 100 ns. The rmsd of **5d** present in the complex exhibited a sudden increase after 30 ns. After that period, the rmsd plot of the bound ligands was consistent throughout the

https://doi.org/10.1021/acsomega.4c00079
ACS Omega 2024, 9, 16384−16399

Table 4. In Silico Docking Results of Synthesized Compounds (5a−5x) against Human Pancreatic α-Amylase (PDB: 6OCN)

code	BA	interacting residues	types of interaction	distance
5a	−8.7	ASP300	conventional H bond	2.27
		ALA198	carbon H bond	2.98
		TRP59	Pi−Pi stacked	4.05, 4.91
		TYR62	Pi−Pi stacked	5.02
5b	−8.1	ARG195	conventional H bond	6.15
		HIS299	carbon H bond	2.83
		TRP59	Pi−Pi stacked	4.73
		TYR62	Pi−Pi stacked	4.27
5c	−9.1	GLN63	conventional H bond	2.54
		HIS299	conventional H bond	2.29
		TRP59	Pi−Pi stacked	4.08, 4.80
		TYR62	Pi−Pi stacked	4.55
		TRP59	Pi-alkyl	5.46
5d	−9.2	SER478	conventional H bond	2.30
		SER437	conventional H bond	4.37
		TRP434	Pi−Pi stacked	5.18
		LEU438	Pi-alkyl	4.94
		TRP434	Pi-alkyl	4.51
5e	−7.8	TRP59	Pi−Pi stacked	4.84, 4.90, 5.81
		LEU165	Pi-alkyl	5.26
5f	−9.1	ASP300	salt bridge	2.15
		ASP300	attractive charge	3.11
		ALA198	carbon H bond	2.84
		TRP59	Pi−Pi stacked	4.04, 4.76
		TYR62	Pi−Pi stacked	5.28
5g	−8.6	SER437	conventional H bond	4.55
		SER478	conventional H bond	2.38
		TRP434	Pi−Pi stacked	5.48
		PHE436	Pi−Pi stacked	5.38
		LEU438	Pi-alkyl	4.76
		TRP434	Pi-alkyl	4.64
5h	−8.2	ASP300	salt bridge	2.97
		ASP300	attractive charge	3.05
		TYR151	conventional H bond	2.55
		ASP197	Pi-anion	4.99
		TRP59	Pi−Pi stacked	4.14, 4.67
		TYR62	Pi−Pi stacked	5.76
5i	−7.7	TRP59	Pi−Pi stacked	4.51, 5.03
		TYR62	Pi−Pi stacked	4.96
		TRP58	Pi−Pi T-shaped	5.33, 5.73
		HIS305	Pi-alkyl	4.86
5j	−8	HIS201	conventional H bond	2.38
		HIS299	conventional H bond	2.43, 2.52
		GLU233	Pi-anion	3.52
		TRP58	Pi-alkyl	5.30
		ILE235	Pi-alkyl	5.02, 5.21
		ALA307	Pi-alkyl	5.05
5k	−8.2	ALA198	carbon H bond	3.06
		ASP300	Pi-anion	4.58
		TRP59	Pi−Pi stacked	4.53, 5.96
		TYR62	Pi−Pi T-shaped	5.01
		LEU162	Pi-alkyl	4.65
5l	−8.3	ARG195	conventional H bond	6.23
		HIS299	carbon H bond	2.87
		ASP300	Pi-anion	4.08
		TRP59	Pi−Pi stacked	4.81, 6.45
		TYR62	Pi−Pi stacked	4.39
		TRP59	Pi-alkyl	4.40
		HIS305	Pi-alkyl	5.45
5m	−8.5	THR163	conventional H bond	2.39
		TYR62	Pi−Pi stacked	4.57
		TRP59	Pi−Pi stacked	3.87
5n	−8.4	ASP300	conventional H bond	2.74
		ASP356	Pi-anion	4.33
		HIS305	Pi−Pi stacked	2.98
		TRP59	Pi−Pi stacked	3.99
		LEU162	Pi-alkyl	5.07
		ALA198	Pi-alkyl	4.91
		TRP59	Pi-alkyl	5.05
5o	−8.1	TRP284	conventional H bond	2.26
		LYS261	carbon H bond	2.70
		LYS261	Pi-cation	4.59, 4.92
		TRP284	Pi−Pi stacked	3.65, 4.83
		LEU237	alkyl, Pi-alkyl	4.41
		LYS257	alkyl, Pi-alkyl	4.85
5p	−8.7	ASP300	conventional H Bond	2.38
		ASP356	Pi-anion	4.16
		HIS305	Pi-sigma	3.00
		TRP59	Pi−Pi stacked	3.97
		ALA198	Pi-alkyl	5.00
		LEU162	Pi-alkyl	5.08
		TRP59	Pi-alkyl	4.06
5q	−8.5	TRP434	Pi−Pi stacked	4.39, 4.84
		LEU438	Pi-alkyl	4.84
5r	−8.3	ASP300	Pi-anion	3.45
		TRP59	Pi−Pi stacked	4.14, 5.28
		ALA198	alkyl, Pi-alkyl	4.39, 4.78
		HIS201	alkyl, Pi-alkyl	4.77
		ILE235	alkyl, Pi-alkyl	5.02
		LEU162	alkyl, Pi-alkyl	5.38, 4.86
5s	−8.4	TRP434	Pi−Pi stacked	5.11
		LEU438	Pi-alkyl	4.89
5t	−8.7	TRP434	Pi−Pi stacked	5.05
		LEU438	Pi-alkyl	4.87
		TRP434	Pi-alkyl	4.53
5u	−7.9	TRP59	Pi−Pi stacked	4.50, 5.02
		TYR62	Pi−Pi stacked	4.98
		TRP58	Pi−Pi T-shaped	5.30, 5.66
		HIS305	Pi-alkyl	4.82
		TRP59	Pi-alkyl	4.85
5v	−9	TRP59	Pi−Pi stacked	4.53, 5.74
		ILE51	alkyl, Pi-alkyl	4.78, 5.01
		VAL107	alkyl, Pi-alkyl	5.23
		LEU165	alkyl, Pi-alkyl	5.36
5w	−8.1	ASP300	conventionalH Bond	2.17
		HIS201	Pi−Pi T-shaped	5.82
		ALA198	alkyl, Pi-alkyl	4.57
		LEU162	alkyl, Pi-alkyl	4.68
		LEU165	alkyl, Pi-alkyl	4.64
		ILE235	alkyl, Pi-alkyl	4.31, 5.16
		ALA307	alkyl, Pi-alkyl	4.92
5x	−7.9	PHE436	Pi−Pi stacked	5.27
		TRP434	Pi−Pi stacked	5.31
		LEU438	alkyl, Pi-alkyl	4.84
		TRP434	alkyl, Pi-alkyl	5.08

https://doi.org/10.1021/acsomega.4c00079
ACS Omega 2024, 9, 16384−16399

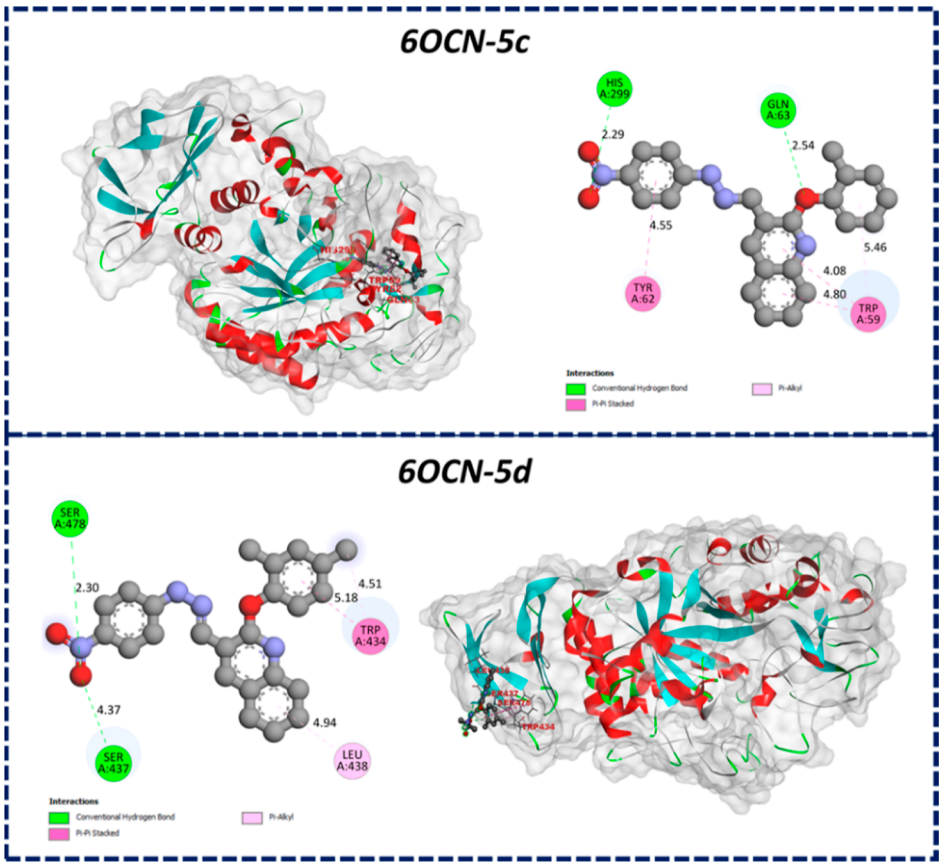

Figure 3. 2D and 3D binding interactions of **5c** and **5d** with targeted α-amylase (PDB: 6OCN).

simulation. This indicated that the complex achieved a stabilized state after 30 ns in its respective structures. The rmsd of Cα (5D41) was less than 2.5 Å, while the rmsd of the hit compound (5d) did not increase above 3.5 Å. The rmsd values plotted in Figure 5 help to indicate prominent scattering in the 6OCN-5d complex. The rmsd profile was used to determine the structural deviations in the docked complex under a real-time simulation. However, further analysis of the MD trajectory involved examining the RMSF profile of Cα atoms within the complex. The resulting RMSF plot illustrated in Figure 6 indicates residual fluctuations across the 100 ns simulation period. Remarkably, the RMSF values for nearly all of the residues remained consistently less than 3.5 Å. This observation indicated the predominantly stable structural behavior of the complex at the residue level. Some amino acid residues present between the 200−250 positions showed fluctuations with sharp peaks in the RMSF plot. However, the values are not much greater than those of the other residues. These findings suggest that the majority of the amino acid residues present in the complex successfully maintain their stability and limit the conformational variability of the 6OCN-5d complex.

Furthermore, interactions within the 6OCN-5d complex during MD simulations were done to estimate the residue-specific engagement with the bound compound **5d**. Analysis of the interactions between the 6OCN residue and compound **5d** elucidated the critical residues governing the binding dynamics. TRP59 was notably involved in the formation of diverse interactions with compound **5d** throughout the 100 ns. Water bridges were formed with the majority of the residues. Figure 7 shows a plot of the fraction of protein−ligand interactions that occurred between specific amino acid residues of 6OCN and compound **5d**. Additionally, ASM53, TRP59, SER108, HIS299, and TRP357 exhibited hydrogen bond formation, highlighting their key roles at the binding interface. The observed binding interactions suggested that the interactions play a crucial role in maintaining the stability and integrity of the 6OCN-5d complex.

CONCLUSIONS

A novel series of phenylhydrazono phenoxyquinoline derivatives (**5a−5x**) were designed and successfully synthesized. In silico studies, including pharmacokinetic profiling, docking, and MD simulation, helped to investigate the biological potential of these synthesized compounds. Compound **5d** was found to be effective against docked α-amylase (PDB 6OCN). A MD simulation study helped to confirm the stability of the docked complex **6OCN-5d** over 100 ns. Moreover, the DFT study successfully indicated that all these compounds have good reactivity. Overall, the findings of the study suggest that synthesized compounds could serve as α-amylase inhibitors after optimization, and the resulting data will help medicinal chemists design.

EXPERIMENTAL SECTION

Materials and Methods. Melting points (mp) reported herein were recorded in open capillary tubes using an Elchem microprocessor-based DT apparatus and were corrected. ^{1}H and ^{13}C NMR spectra were acquired using Bruker 400 MHz spectrometers, employing tetramethylsilane (TMS) as an internal reference, and chemical shift values were expressed in parts per million (ppm). High-resolution mass spectra were

https://doi.org/10.1021/acsomega.4c00079
ACS Omega 2024, 9, 16384−16399

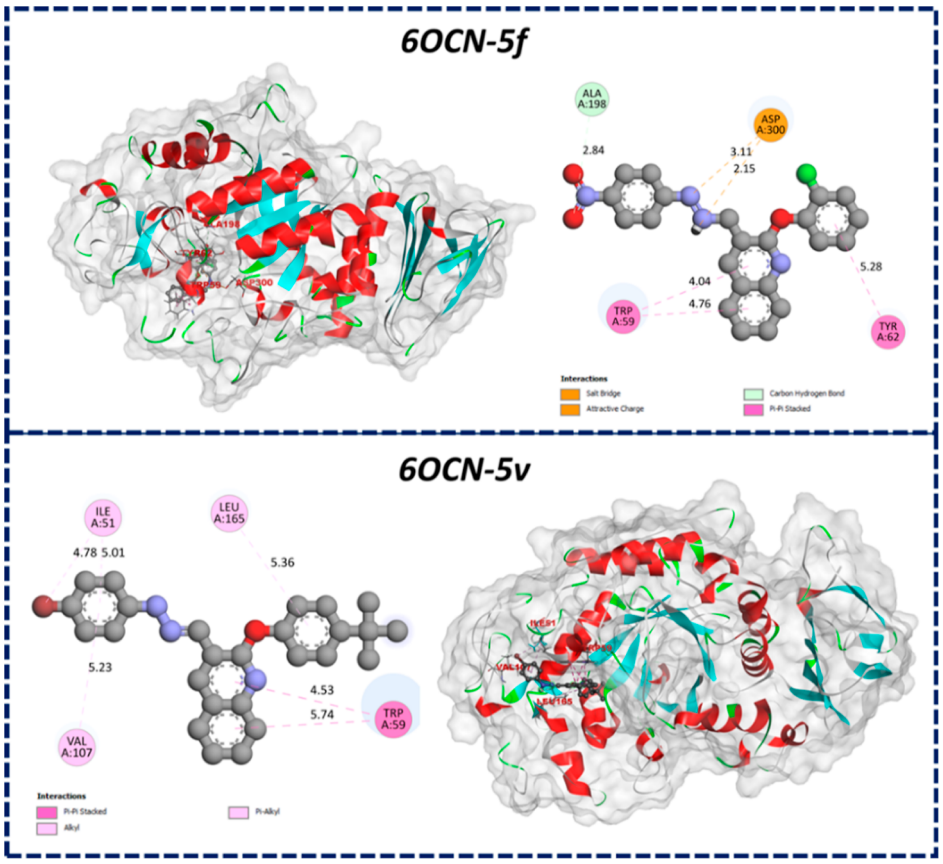

Figure 4. 2D and 3D binding interactions of **5f** and **5v** with targeted α-amylase (PDB: 6OCN).

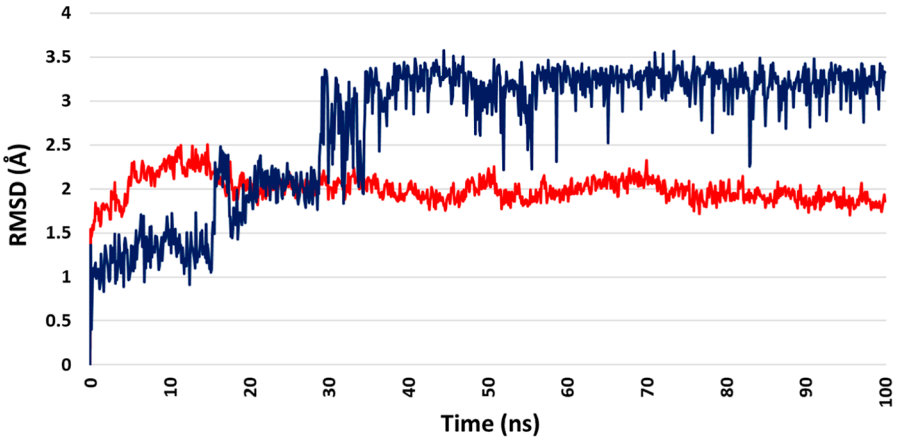

Figure 5. RMSD plot for Cα structures from α-amylase (red) and the bound hit ligand (blue).

obtained by using a Bruker MaXis HR-MS (ESI-Q-TOF−MS) instrument. All reagents were purchased from Aldrich and used as received. Solvents were removed under a vacuum. Organic extracts were dried with anhydrous Na_2SO_4. Analytical thin-layer chromatography (TLC) was performed using silica gel $60F_{254}$ aluminum sheets. Visualization of spots on TLC plates was achieved through ultraviolet (UV) illumination, exposure to iodine vapor, and heating the plates dipped in $KMnO_4$ stain. Silica gel with a 230−400 mesh size was used for purification via column chromatography.

Synthesis of Phenylhydrazono Phenoxyquinoline Derivatives (5a-5x). The synthetic work was carried out using 2-chloro-3-formyl quinoline **1** as the starting material, as shown in Scheme 1. The reaction of 2-chloro-3-formyl quinoline (**1**) with phenol derivatives (**2a−2l**) in the presence of K_2CO_3/DMF at 100 °C for 1 h yielded substituted 2-phenoxyquinoline-3-carbaldehyde (**3a−3l**). This intermediate further reacted with the 4-bromo/nitro phenylhydrazine (**4a−4b**), resulting in corresponding 3-((2-(4-nitro/bromo phenyl) hydrazono) methyl)-2-phenoxyquinoline (**5a−5x**), which was subsequently treated with acetic acid in methanol at 65 °C for 30 min. The reaction mixture was then poured into chilled water, filtered, and recrystallized using EtOH. All the newly synthesized novel compounds were characterized by analytical tools (^{1}H NMR, ^{13}C NMR, and HRMS).

https://doi.org/10.1021/acsomega.4c00079
ACS Omega 2024, 9, 16384−16399

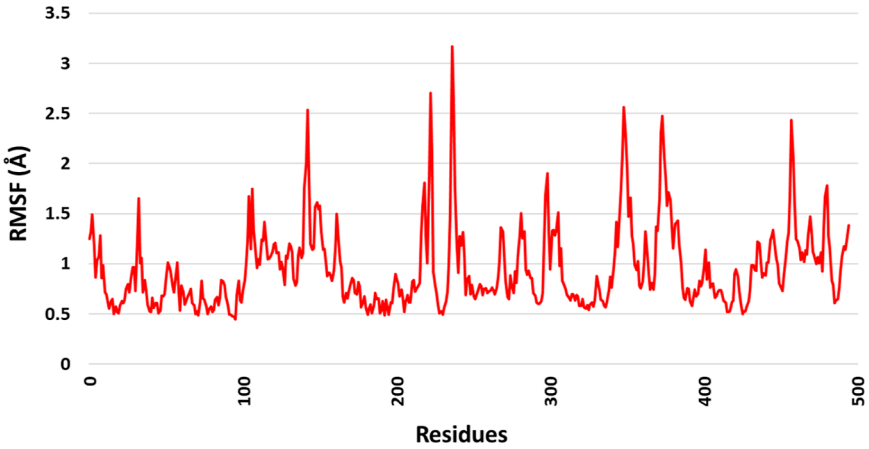

Figure 6. RMSF plot of Cα from the 6OCN-5d complex simulated for 100 ns.

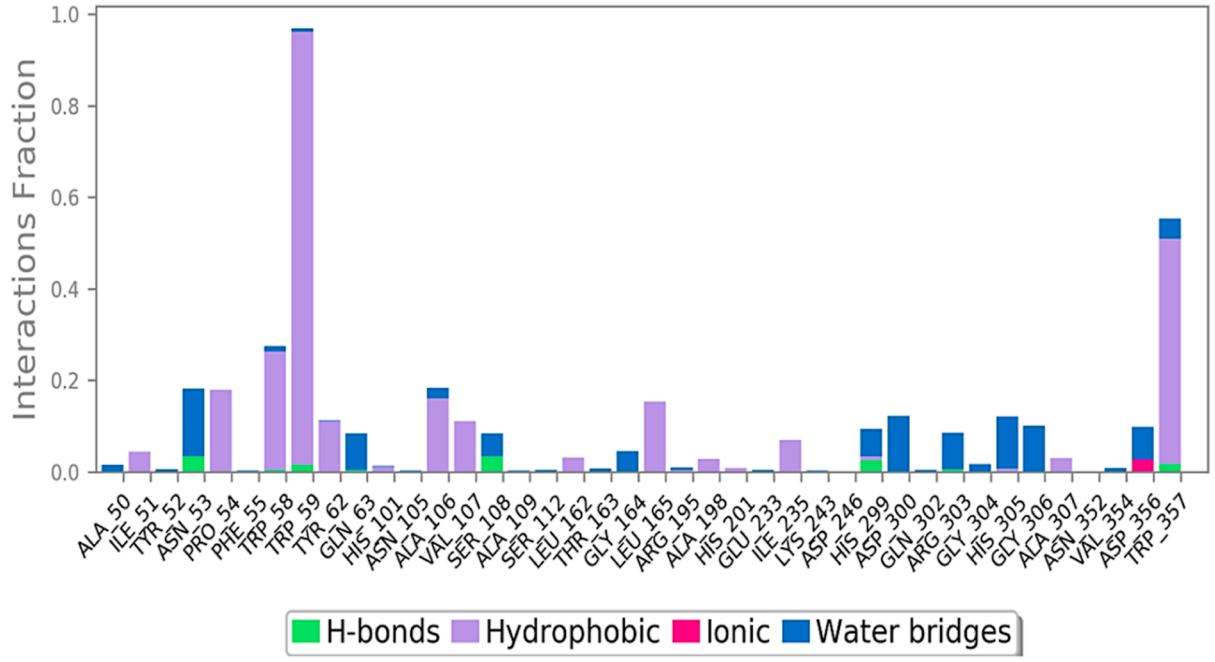

Figure 7. Fraction of interactions formed between α-amylase (PDB 6OCN) and compound **5d** over 100 ns MD simulation.

*3-((2-(4-Nitrophenyl)hydrazono)methyl)-2-phenoxyquinoline (**5a**).* Orange solid. Yield 82%. mp 255−257 °C. ^{1}H NMR (400 MHz, DMSO−d_6): δ 11.63 (s,1H), 8.95 (s,1H), 8.53(s,1H), 8.13 (d, *J* = 9.6 Hz, 2H), 8.078 (d, *J* = 8 Hz, 1H), 7.67−7.63 (m, 1H), 7.59 (d, *J* = 8.4 Hz, 1H), 7.53−7.47 (m, 3H), 7.32−7.27 (m,5H). ^{13}C NMR (100 MHz, DMSO-d_6): δ ppm 159.00, 153.82, 150.68, 145.77, 139.77, 135.96, 134.85, 130.90, 130.13, 128.89, 127.27, 126.64, 126.25, 125.97, 125.43, 122.19, 119.92, 112.11. HRMS-ESI (*m*/*z*): calcd for $C_{22}H_{16}N_4O_3$ [M]$^+$, 384.1222, observed = 384.1220.

*3-((2-(4-Nitrophenyl)hydrazono)methyl)-2-(o-tolyloxy)-quinoline (**5b**).* Orange solid. Yield 85%. mp 261−263 °C. ^{1}H NMR (400 MHz, DMSO−d_6): δ 11.64 (s,1H), 8.95 (s,1H), 8.58 (s, 1H), 8.19 (d, *J* = 9.2 Hz, 2H), 8.07 (d, *J* = 8 Hz, 1H), 7.63 (t, *J* = 7.4 Hz, 1H), 7.49 (t, *J* = 7.2 Hz, 1H), 7.37 (d, *J* = 7.6 Hz, 1H), 7.33−7.20 (m, 5H), 2.15 (s, 1H). ^{13}C NMR (100 MHz, DMSO-d_6): δ ppm 158.72, 152.06, 150.58, 145.86, 139.38, 135.93, 134.84, 131.64, 130.88, 130.58, 128.91, 127.64, 127.21, 126.65, 126.11, 125.84, 125.80, 122.83, 119.55, 112.12, 16.57. HRMS-ESI (*m*/*z*): calcd for $C_{23}H_{18}N_4O_3$ [M]$^+$, 398.1379, observed = 398.1376.

*3-((2-(4-Nitrophenyl)hydrazono)methyl)-2-(p-tolyloxy)-quinoline (**5c**).* Orange solid. Yield 76%. mp 267−269 °C. ^{1}H NMR (400 MHz, DMSO−d_6): δ 11.62 (s,1H), 8.92 (s,1H), 8.52 (s,1H), 8.18 (d, *J* = 9.2 Hz, 2H), 8.05 (d, *J* = 8 Hz, 1H), 7.64 (t, *J* = 7.6 Hz, 1H), 7.27 (d, *J* = 7.6 Hz, 4H), 7.18 (d, *J* = 8.4 Hz, 2H), 2.36 (s, 3H). ^{13}C NMR (100 MHz, DMSO-d_6): δ ppm 159.16, 151.49, 150.68, 145.81, 139.37, 136.02, 134.73, 134.49, 130.85, 130.49, 128.85, 127.23, 126.62, 126.16, 125.87, 121.99, 119.85, 112.10, 20.92. HRMS-ESI (*m*/*z*): calcd for $C_{23}H_{18}N_4O_3$ [M]$^+$, 398.1379, observed = 398.1375.

*2-(2,4-Dimethylphenoxy)-3-((2-(4-nitrophenyl)-hydrazono)methyl)quinoline (**5d**).* Orange solid. Yield 75%. mp 272−274 °C. ^{1}H NMR (400 MHz, DMSO−d_6): δ 11.64 (s, 1H), 8.93 (s,1H), 8.58 (s,1H), 8.19 (d, *J* = 9.6 Hz, 2H), 8.05 (d, *J* = 8 Hz, 1H), 7.64−7.60 (m, 1H), 7.54 (d, *J* = 8.4 Hz, 1H), 7.48 (t, *J* = 36.4 Hz, 1H), 7.28 (d, *J* = 8.4 Hz, 2H), 7.16 (s, 1H), 7.10 (s, 2H), 2.33 (s, 3H) 2.09 (s, 3H). ^{13}C NMR (100 MHz, DMSO-d_6): δ ppm 158.84, 150.67, 149.76, 145.90,

https://doi.org/10.1021/acsomega.4c00079
ACS Omega 2024, 9, 16384−16399

139.35, 135.96, 134.76, 134.72, 132.11, 130.85, 130.18, 128.89, 128.05, 127.18, 126.65, 126.04, 125.76, 122.60, 119.49, 112.10. HRMS-ESI (m/z): calcd for $C_{24}H_{20}N_4O_3$ $[M]^+$, 412.1535, observed = 412.1533.

*2-(2-Chlorophenoxy)-3-((2-(4-nitrophenyl)hydrazono)-methyl)quinoline (**5e**).* Orange solid. Yield 89%. mp 282−284 °C. ^{1}H NMR (400 MHz, DMSO−d_6): δ 11.67 (s, 1H), 8.98 (s, 1H), 8.57 (s, 1H), 8.19 (d, J = 9.6 Hz, 2H), 8.06 (d, J = 8 Hz, 1H), 7.63 (t, J = 7.5 Hz, 1H), 7.55 (d, J = 8 Hz, 1H), 7.49 (t, J = 7.4 Hz, 1H), 7.29 (d, J = 8 Hz, 2H). ^{13}C NMR (100 MHz, DMSO-d_6): δ ppm 158.28, 150.65, 145.56, 139.47, 135.51, 135.10, 131.05, 130.81, 129.05, 128.96, 127.43, 127.43, 127.28, 126.64, 126.35, 126.15, 125.26, 119.38, 112.19. HRMS-ESI (m/z): calcd for $C_{22}H_{15}ClN_4O_3$ $[M]^+$, 418.0833, observed = 418.0830.

*2-(3-Chlorophenoxy)-3-((2-(4-nitrophenyl)hydrazono)-methyl)quinoline (**5f**).* Orange solid. Yield 70%. mp 285−287 °C. ^{1}H NMR (400 MHz, DMSO−d_6): δ 11.64 (s, 1H), 8.96 (s, 1H), 8.48 (s, 1H), 8.13 (d, J = 36.8 Hz, 3H), 7.45 (dd, J = 44.8−34 Hz, 8H). ^{13}C NMR (100 MHz, DMSO-d_6): δ ppm 158.70, 154.59, 150.65, 145.59, 139.39, 135.74, 135.04, 133.95, 131.54, 131.01, 128.91, 127.33, 126.64, 126.40, 126.18, 125.62, 122.58, 121.22, 119.86, 122.13. HRMS−ESI (m/z): calcd for $C_{22}H_{15}ClN_4O_3$ $[M]^+$, 418.0833, observed = 418.0831.

*2-(4-Chlorophenoxy)-3-((2-(4-nitrophenyl)hydrazono)-methyl)quinoline (**5g**).* Orange solid. Yield 92%. mp 286−289 °C. ^{1}H NMR (400 MHz, DMSO−d_6): δ 11.64 (s, 1H), 8.96 (s, 1H), 8.52 (s, 1H), 8.19 (d, J = 8.8 Hz, 2H), 8.09 (d, J = 8 Hz, 1H), 7.68−7.60 (m, 2H), 7.53 (q, J = 13.6−12.8 Hz, 3H), 7.37 (d, J = 8.8 Hz, 2H), 7.28 (d, J = 8.4 Hz, 2H). ^{13}C NMR (100 MHz, DMSO-d_6): δ ppm 159.17, 151.47, 150.68, 145.80, 139.35, 136.01, 134.76, 134.53, 130.90, 130.51, 128.87, 127.23, 126.65, 125.90, 122.01, 119.84, 112.12. HRMS-ESI (m/z): calcd for $C_{22}H_{15}ClN_4O_3$ $[M]^+$, 418.0833, observed = 418.0829.

*2-(2,4-Dichlorophenoxy)-3-((2-(4-nitrophenyl)-hydrazono)methyl)quinoline (**5h**).* Orange solid. Yield 83%. mp 293−295 °C. ^{1}H NMR (400 MHz, DMSO−d_6): δ 8.98 (s, 1H), 8.54 (s, 1H), 8.18 (d, J = 8.8 Hz, 2H), 8.09 (d, J = 8 Hz, 1H), 7.81 (d, J = 8.8 Hz, 2H), 8.09 (d, J = 8 Hz, 1H), 7.81 (t, J = 17.6 Hz, 1H), 7.65 (t, J = 14.8 Hz, 1H), 7.57−7.49 (m, 4H), 7.34−7.21 (m,3H). ^{13}C NMR (100 MHz, DMSO-d_6): δ ppm 172.51, 162.15, 158.44, 150.88, 148.43, 146.10, 143.07, 136.68, 131.81, 130.86, 130.32, 129.43, 129.21, 127.93, 127.28, 126.66, 126.36, 126.16, 118.55. HRMS-ESI (m/z): calcd for $C_{22}H_{14}Cl_2N_4O_3$ $[M]^+$, 452.0443, observed = 452.0440.

*2-(4-Bromophenoxy)-3-((2-(4-nitrophenyl)hydrazono)-methyl)quinoline (**5i**).* Orange solid. Yield 78%. mp 297−300 °C. ^{1}H NMR (400 MHz, DMSO−d_6): δ 11.64 (s, 1H), 8.96 (s, 1H), 8.51 (s, 1H), 8.13 (dd, J = 41.2−40 Hz, 3H), 7.62 (q, J = 22.4−39.6 Hz, 5H), 7.318 (d, J = 8 Hz, 4H). ^{13}C NMR (100 MHz, DMSO-d_6): δ ppm 162.04, 159.15, 152.95, 150.88, 146.28, 143.44, 140.61, 136.38, 133.02, 131.65, 129.37, 127.28, 126.18, 126.08, 124.73, 122.01, 119.12, 117.74. HRMS-ESI (m/z): calcd for $C_{22}H_{15}BrN_4O_3$ $[M]^+$, 462.0328, observed = 462.0325.

*2-(4-(tert-Butyl)phenoxy)-3-((2-(4-nitrophenyl)-hydrazono)methyl)quinoline (**5j**).* Orange solid. Yield 74%. mp 277−279 °C. ^{1}H NMR (400 MHz, DMSO−d_6): δ 11.64 (s, 1H), 8.93 (s, 1H), 8.50 (s, 1H), 8.18 (d, J = 9.2 Hz, 2H), 8.06 (d, J = 8 Hz, 1H), 7.66−7.59 (m, 2H), 7.52−7.47 (m, 3H), 7.28 (d, J = 8.4 Hz, 2H), 7.24 (d, J = 8.8 Hz, 2H), 1.34 (s, 9H). ^{13}C NMR (100 MHz, DMSO-d_6): δ ppm 158.99, 151.47, 150.70, 147.57, 145.80, 139.37, 135.94, 134.86, 130.89, 128.88, 127.44, 126.78, 126.63, 126.63, 126.21, 125.93, 121.47, 119.96, 112.13, 31.77. HRMS-ESI (m/z): calcd for $C_{26}H_{24}N_4O_3$ $[M]^+$, 440.1848, observed = 440.1845.

*3-((2-(4-Nitrophenyl)hydrazono)methyl)-2-(m-tolyloxy)-quinoline (**5k**).* Orange solid. Yield 87%. mp 256−258 °C. ^{1}H NMR (400 MHz, DMSO−d_6): δ 11.64 (s, 1H), 8.95 (s, 1H), 8.58 (s, 1H), 8.19 (d, J = 9.2 Hz, 2H), 8.07 (d, J = 8 Hz, 1H), 7.62 (t, J = 14.8 Hz, 1H), 7.55−7.48 (m, 2H), 7.37 (d, J = 7.6 Hz, 1H), 7.33−7.20 (m, 5H), 2.14 (s, 3H). ^{13}C NMR (100 MHz, DMSO-d_6): δ ppm 158.72, 152.06, 150.68, 145.86, 139.38, 135.93, 134.84, 131.64, 130.88, 130.58, 128.91, 127.64, 127.21, 126.65, 126.11, 125.84, 125.80, 122.83, 119.55, 112.12, 16.57. HRMS-ESI (m/z): calcd for $C_{23}H_{18}N_4O_3$ $[M]^+$, 398.1379, observed = 398.1377.

*2-(2,6-Dimethoxyphenoxy)-3-((2-(4-nitrophenyl)-hydrazono)methyl)quinoline (**5l**).* Orange solid. Yield 77%. mp 276−278 °C. ^{1}H NMR (400 MHz, DMSO−d_6): δ 11.67 (s, 1H), 8.89 (s, 1H), 8.59 (s, 1H), 8.19 (d, J = 5.6 Hz, 1H), 8.02 (q, J = 17.6−18 Hz, 1H), 7.60 (t, J = 15.2 Hz, 1H),7.53−7,44 (m, 3H), 7.30−7.17 (m, 3H), 6.81 (q, J = 14−14 Hz, 2H), 3.70 (s, 6H). ^{13}C NMR (100 MHz, DMSO-d_6): δ ppm 158.80, 158.44, 153.05, 150.70, 145.97, 139.37, 137.53, 136.14, 134.42, 130.57, 128.89, 127.15, 126.97, 126.64, 126.16, 125.59, 119.13, 112.13, 106.18, 106.02, 56.52, 56.47. HRMS-ESI (m/z): calcd for $C_{24}H_{20}N_4O_5$ $[M]^+$, 444.1434, observed = 444.1431.

*(2-(4-Bromophenyl)hydrazono)methyl)-2-phenoxyquinoline (**5m**).* Reddish brown solid. Yield 71%. mp 288−291 °C. ^{1}H NMR (400 MHz, DMSO−d_6): δ 11.53 (s, 1H), 8.85 (s, 1H), 8.43 (s, 1H), 8.08 (d, J = 9.6 Hz, 2H), 7.97 (d, J = 8 Hz, 1H), 7.57−7.53 (m, 1H), 7.49 (d, J = 8.4 Hz, 1H), 7.43−7.37 (m, 3H), 7.22−7.19 (m, 5H). ^{13}C NMR (100 MHz, DMSO-d_6): δ ppm 157.00, 151.82, 148.68, 143.77, 137.37, 133.96, 132.85, 128.90, 128.13, 126.89, 125.27, 124.64, 124.25, 123.97, 123.43, 120.19, 117.92, 110.11. HRMS-ESI (m/z): calcd for $C_{22}H_{16}BrN_3O$ $[M]^+$, 417.0477, observed = 417.0475.

*3-((2-(4-Bromophenyl)hydrazono)methyl)-2-(o-tolyloxy)-quinoline (**5n**).* Reddish brown solid. Yield 73%. mp 295−298 °C. ^{1}H NMR (400 MHz, DMSO−d_6): δ 11.64 (s, 1H), 8.95 (s, 1H), 8.58 (s, 1H), 8.19 (d, J = 9.2 Hz, 2H), 8.07 (d, J = 8 Hz, 1H), 7.63 (t, J = 14.4 Hz, 1H), 7.56−7.48 (m, 2H), 7.37 (d, J = 7.2 Hz, 1H), 7.31−7.22 (m, 5H), 2.14 (s, 3H). ^{13}C NMR (100 MHz, DMSO-d_6): δ ppm 158.75, 152.09, 150.71, 145.89, 139.97, 134.87, 131.67, 130.91, 130.61, 128.94, 127.67, 127.24, 126.68, 126.14, 125.83, 122.86, 119.58, 112.15, 16.60. HRMS-ESI (m/z): calcd for $C_{23}H_{18}BrN_3O$ $[M]^+$, 431.0633, observed = 431.0630.

*3-((2-(4-Bromophenyl)hydrazono)methyl)-2-(p-tolyloxy)-quinoline (**5o**).* Reddish brown solid. Yield 78%. mp 302−304 °C. ^{1}H NMR (400 MHz, DMSO−d_6): δ 11.39 (s, 1H), 8.69 (s, 1H), 8.29 (s, 1H), 7.95 (d, J = 9.2 Hz, 2H), 7.83 (d, J = 8 Hz, 1H), 7.41 (t, J = 15.2 Hz, 1H), 7.35 (d, J = 8.4 Hz, 1H), 7.27 (t, J = 14.8 Hz, 1H), 7.05 (d, J = 8 Hz, 4H), 6.95 (d, J = 8.4 Hz, 2H), 2.14 (s, 3H). ^{13}C NMR (100 MHz, DMSO-d_6): δ ppm 159.16, 151.49, 150.68, 145.81, 139.37, 136.02, 134.73, 134.49, 130.85, 130.49, 128.85, 127.23, 126.62, 126.16, 125.87, 121.99, 119.85, 112.10, 20.92. HRMS-ESI (m/z): calcd for $C_{23}H_{18}BrN_3O$ $[M]^+$, 431.0633, observed = 431.0629.

*3-((2-(4-Bromophenyl)hydrazono)methyl)-2-(2,4-dimethylphenoxy)quinoline (**5p**).* Reddish brown solid. Yield 81%. mp 307−309 °C. ^{1}H NMR (400 MHz, DMSO−d_6): δ 11.70 (s, 1H), 8.98 (s, 1H), 8.63 (s, 1H), 8.25 (d, J = 9.2 Hz,

https://doi.org/10.1021/acsomega.4c00079
ACS Omega 2024, 9, 16384−16399

2H), 8.12 (d, J = 8 Hz, 1H), 7.70−7.66 (m, 1H), 7.60 (d, J = 8 Hz, 1H), 7.54 (t, J = 15.6 Hz, 1H), 7.34 (d, J = 8.4 Hz, 2H), 7.22 (s, 1H), 7.16 (s, 2H), 2.39 (s, 3H), 2.15 (s, 3H). ^{13}C NMR (100 MHz, DMSO-d_6): δ ppm 159.84, 151.67, 150.76, 146.90, 140.35, 136.98, 135.76, 135.72, 133.11, 131.85, 131.18, 129.89, 129.05, 128.18, 127.65, 127.04, 126.76, 123.60, 120.49, 113.10, 21.92, 17.52. HRMS-ESI (m/z): calcd for $C_{24}H_{20}BrN_3O$ $[M]^+$, 445.0790, observed = 445.0788.

*3-((2-(4-Bromophenyl)hydrazono)methyl)-2-(2-chlorophenoxy)quinoline (**5q**).* Reddish brown solid. Yield 70%. mp 311−313 °C. ^{1}H NMR (400 MHz, DMSO−d_6): δ 11.57 (s, 1H), 8.88 (s, 1H), 8.47 (s, 1H), 8.09 (d, J = 8.8 Hz, 2H), 7.99 (d, J = 8 Hz, 1H), 7.54 (t, J = 13.2 Hz, 2H), 7.47−7.37 (m, 4H), 7.28−7.18 (m, 3H). ^{13}C NMR (100 MHz, DMSO-d_6): δ ppm 158.28, 150.65, 145.56, 139.47, 135.10, 131.05, 130.81, 129.05, 128.96, 127.43, 127.28, 126.64, 126.35, 126.15, 125.65, 119.38, 112.19. HRMS-ESI (m/z): calcd for $C_{22}H_{15}Cl$ BrN_3O $[M]^+$, 451.0087, observed = 451.0085.

*3-((2-(4-Bromophenyl)hydrazono)methyl)-2-(3-chlorophenoxy)quinoline (**5r**).* Reddish brown solid. Yield 73%. mp 312−315 °C. ^{1}H NMR (400 MHz, DMSO−d_6): δ 12.45 (s, 1H), 9.05 (d, J = 15.2HZ, 2H), 8.90 (s, 2H), 8.23 (d, J = 8 Hz, 1H), 7.97 (d, J = 4.4 Hz, 2H), 7.80−7.71 (m, 2H), 7.61 (t, J = 17.2 Hz, 3H), 7.44 (q, J = 17.6−18 Hz, 2H). ^{13}C NMR (100 MHz, DMSO-d_6): δ ppm 159.68, 155.59, 151.65, 146.59, 140.39, 136.73, 136.05, 134.95, 132.54, 132.02, 129.92, 128.32, 127.63, 126.62, 123.56, 122.21, 120.85, 113.13. HRMS-ESI (m/z): calcd for $C_{22}H_{15}Cl$ BrN_3O $[M]^+$, 451.0087, observed = 451.0086.

*3-((2-(4-Bromophenyl)hydrazono)methyl)-2-(4-chlorophenoxy)quinoline (**5s**).* Reddish brown solid. Yield 76%. mp 317−319 °C. ^{1}H NMR (400 MHz, DMSO−d_6): δ 12.41 (s, 1H), 9.06 (s, 1H), 9.01 (s, 1H), 8.87 (d, J = 4 Hz, 2H), 8.21 (d, J = 8 Hz, 1H), 7.95 (d, J = 5.6 Hz, 2H), 7.76 (t, J = 14.4 Hz, 1H), 7.69 (d, J = 8.4 Hz, 1H), 7.62 (d, J = 8.8 Hz, 3H), 7.45(d, J = 8.8 Hz, 2H). ^{13}C NMR (100 MHz, DMSO-d_6): δ ppm 159.17, 151.47, 150.68, 145.80, 139.35, 136.01, 134.76, 134.53, 130.90, 130.51, 128.87, 127.23, 126.65, 126.15, 125.90, 122.01, 119.84, 112.12. HRMS-ESI (m/z): calcd for $C_{22}H_{15}Cl$ BrN_3O $[M]^+$, 451.0087, observed = 451.0084.

*3-((2-(4-Bromophenyl)hydrazono)methyl)-2-(2,4-dichlorophenoxy)quinoline (**5t**).* Reddish brown solid. Yield 77%. mp 320−323 °C. ^{1}H NMR (400 MHz, DMSO−d_6): δ 9.07 (s, 1H), 8.63 (s, 1H), 8.26 (t, J = 21.2 Hz, 2H), 8.18 (d, J = 8 Hz, 1H), 7.91 (t, J = 17.6 Hz, 1H), 7.80 (t, J = 14.8 Hz, 1H), 7.68−7.60 (m, 4H), 7.34 (q, J = 24.8−23.2 Hz, 3H). ^{13}C NMR (100 MHz, DMSO-d_6): δ ppm 173.61, 163.25, 159.54, 151.98, 149.53, 147.20, 144.17, 137.78, 132.91, 131.91, 131.42, 130.53, 130.31, 129.03, 128.38, 127.76, 127.46, 127.26, 119.65. HRMS-ESI (m/z): calcd for $C_{22}H_{14}Cl_2N_3O$ $[M]^+$, 484.9697, observed = 484.9695.

*2-(4-Bromophenoxy)-3-((2-(4-bromophenyl)hydrazono)-methyl)quinoline (**5u**).* Reddish brown solid. Yield 74%. mp 331−333 °C. ^{1}H NMR (400 MHz, DMSO−d_6): δ 11.40 (s, 1H), 8.72 (s, 1H), 8.27 (s, 1H), 7.89 (dd, J = 41.2−40 Hz, 3H), 7.38 (q, J = 22.8−55.8 Hz, 5H), 7.07 (d, J = 8 Hz, 4H). ^{13}C NMR (100 MHz, DMSO-d_6): δ ppm 163.03, 160.14, 153.94, 151.87, 147.27, 144.43, 141.60, 137.37, 134.01, 132.64, 130.36, 128.27, 127.17, 127.07, 125.72, 123.00, 120.11, 118.73. HRMS-ESI (m/z): calcd for $C_{22}H_{15}Br_2N_3O$ $[M]^+$, 494.9582, observed = 494.9580.

*3-((2-(4-Bromophenyl)hydrazono)methyl)-2-(4-(tert-butyl)phenoxy)quinoline (**5v**).* Reddish brown solid. Yield 72%. mp 313−316 °C. ^{1}H NMR (400 MHz, DMSO−d_6): δ 11.70 (s, 1H), 8.99 (s, 1H), 8.56 (s, 1H), 8.24 (d, J = 9.6 Hz, 2H), 8.12 (d, J = 8 Hz, 1H), 7.72−7.64 (m, 2H), 7.55 (t, J = 18 Hz, 3H), 7.33 (d, J = 8.4 Hz, 2H), 7.27 (d, J = 8.4 Hz, 2H), 1.39 (s, 9H). ^{13}C NMR (100 MHz, DMSO-d_6): δ ppm 158.99, 151.47, 150.70, 147.57, 145.80, 139.37, 135.94, 134.86, 130.89, 128.88, 127.24, 126.78, 126.63, 126.21, 125.93, 121.47, 119.96, 112.13, 34.69, 31.77. HRMS-ESI (m/z): calcd for $C_{26}H_{24}BrN_3O$ $[M]^+$, 473.1179, observed = 473.1180.

*3-((2-(4-Bromophenyl)hydrazono)methyl)-2-(m-tolyloxy)-quinoline (**5w**).* Reddish brown solid. Yield 80%. mp 303−305 °C. ^{1}H NMR (400 MHz, DMSO−d_6): δ 11.74 (s, 1H), 9.05 (s, 1H), 8.68 (s, 1H), 8.29 (d, J = 9.2 Hz, 2H), 8.17 (d, J = 8 Hz, 1H), 7.72 (t, J = 14.8 Hz, 1H), 7.65−7.58 (m, 2H), 7.47 (d, J = 7.6 Hz, 1H), 7.41−7.32 (m, 5H), 2.24 (s, 3H). ^{13}C NMR (100 MHz, DMSO-d_6): δ ppm 157.75, 151.09, 149.71, 144.89, 138.41, 134.97, 133.87, 130.67, 129.61, 127.94, 126.67, 126.24, 125.68, 124.87, 121.86, 118.58, 111.15, 15.60. HRMS-ESI (m/z): calcd for $C_{23}H_{18}BrN_3O$ $[M]^+$, 431.0633, observed = 431.0631.

*3-((2-(4-Bromophenyl)hydrazono)methyl)-2-(2,6-dimethoxyphenoxy)quinoline (**5x**).* Reddish brown solid. Yield 79%. mp 308−312 °C. ^{1}H NMR (400 MHz, DMSO−d_6): δ 11.49 (s, 1H), 8.72 (s, 1H), 8.41 (s, 1H), 8.02 (d, J = 8.8 Hz, 2H), 7.84 (dd, J = 18−18 Hz, 1H), 7.43 (t, J = 14.8 Hz, 2H), 7.32 (q, J = 15.6−14.8 Hz, 2H), 7.09 (q, J = 18−18.4 Hz, 2H), 6.65 (t, J = 14 Hz, 2H), 3.52 (S, 6H). ^{13}C NMR (100 MHz, DMSO-d_6): δ ppm 159.44, 154.05, 151.70, 146.97, 140.37, 138.53, 137.14, 135.42, 131.78, 129.89, 128.15, 127.64, 127.16, 126.59, 123.26, 120.13, 113.13, 107.02, 57.47. HRMS-ESI (m/z): calcd for $C_{24}H_{20}BrN_3O_3$ $[M]^+$, 477.0688, observed = 477.0686.

Computational Studies. *Ligand Preparation.* The chemical structures of synthesized phenylhydrazono phenoxyquinoline derivatives (**5a−5x**) were generated using ACD/ChemSketch software.[29] BIOVIA Discovery Studio was used to protonate the sketched chemical structures of synthesized phenylhydrazono phenoxyquinoline derivatives (**5a−5x**).[30] The prepared chemical structures were then energy minimized and optimized employing the steepest descent algorithm and the MMFF94 force field.[25,31] Ligand structure optimization was performed using the OpenBabel module from PyRx 0.8.[32,33]

Drug-Likeness and In Silico ADMET Prediction. The drug-likeness and pharmacokinetic (ADMET) profiles of the synthesized phenylhydrazono phenoxyquinoline derivatives (**5a-5x**) were estimated utilizing the online SwissADME and pkCSM servers.[34,35] Various criteria from a set of rules, including Lipinski's rule (Ro5), Veber's rule, Ghose's rule, Egan's rule, and Muegge's rule, were considered to estimate the drug-likeness profile of synthesized phenylhydrazono phenoxyquinoline derivatives (**5a−5k**).[36−40]

Density Functional Theory Calculations. The energies of FMOs and chemical reactivity descriptors based on FMOs for synthesized phenylhydrazono phenoxyquinoline derivatives (**5a−5x**) were calculated utilizing the DFT method.[25,26,41] Previously reported protocols were followed for carrying out the DFT calculations.[22,24,42] The B3LYP/DEF2-SVP level of theory and the ORCA 5.0.4 program were employed for the execution of all the DFT calculations.[43−48] Input and output files were generated on orca-enhanced Avogadro software.[48,49] The chemical reactivity descriptors were calculated with previously reported equations from Koopmans' theory.[50,51]

https://doi.org/10.1021/acsomega.4c00079
ACS Omega 2024, 9, 16384−16399

Molecular Docking Study. *Target Protein Retrieval and Preparation.* Crystallographic structures of human pancreatic α-amylase (PDB ID: 6OCN, resolution 1.15 Å) were downloaded from the RCSB Protein Data Bank.[52] These structures underwent rigorous optimization and minimization procedures employing AutoDockVina tools and BIOVIA Discovery Studio.[30,53] The optimization process included tasks such as filling in missing residues, side chain generation, and hydrogen atom addition.[54,55] Additionally, the histidine residues were assigned appropriate protonation states, and charges were incorporated for both standard and nonstandard residues, ensuring net charge stabilization. Nonstandard residues, water molecules, cocrystal ligands, and extraneous chains were systematically removed using BIOVIA Discovery Studio to streamline the protein structures for subsequent investigations.[56−58]

Docking of Ligands with the Target Protein. Docking studies were conducted using the AutoDock Vina module in PyRx 0.8 with a maximized grid spacing.[31,33,59,60] Initially, protein structures obtained from the RCSB Protein Data Bank were thoroughly cleaned, with prior ligands and water molecules. Polar hydrogen atoms were added, and the structures were optimized using BIOVIA Discovery Studio, ensuring accurate tautomeric states.[61] Following energy minimization, ligand and protein structures were chosen for the docking study in Vina Wizard, with a maximized grid box covering the entire protein. Parameters such as exhaustiveness at eight and the number of modes at nine were configured for the study.[23] The docking data were subsequently analyzed with the BIOVIA Discovery Studio visualizer, providing valuable insights into protein−ligand interactions.[30] This rigorous computational approach integrates advanced tools and protocols to comprehensively investigate molecular interactions with precision.

MD Simulation. MD simulation of the hit compound was carried out using Desmond 2020.1 software. MD simulation was performed with the OPLS-2005 force field.[62] The complex was solvated in an orthorhombic box with TIP3P water molecules. The explicit solvent model was used for solvation.[63] Periodic boundary conditions were set as dimensions of 10 Å × 10 Å × 10 Å to enclose the protein−ligand complex in a water box.[63−67] The physiological surroundings in the water box achieved by the addition of NaCl atoms and charges were counterbalanced with 0.15 M Na^+ ions. Equilibration of the complex was performed for the initial 10 ns with the *NVT* ensemble.[68] The *NPT* ensemble for a duration of the next 12 ns was achieved for brief equilibration and energy minimization of the complex.[69] A pressure of 1 bar with a relaxation time of 1.0 ps was maintained via the Nose−Hoover chain coupling approach.[70] The barostat method was applied to control the pressure.[71] A production run was completed for a period of 100 ns. The resulting MD trajectories were statistically analyzed.[72,73]

■ ASSOCIATED CONTENT

Supporting Information

The Supporting Information is available free of charge at https://pubs.acs.org/doi/10.1021/acsomega.4c00079.

^{1}HNMR, ^{13}CNMR, and HRMS spectra data of synthesized compounds (PDF)

■ AUTHOR INFORMATION

Corresponding Authors

Imadul Islam − *King Abdullah International Medical Research Center (KAIMRC), King Saud Bin Abdulaziz University for Health Sciences, Ministry of National Guard-Health Affairs, Riyadh 14811, Saudi Arabia*; Email: imadulislam@yahoo.com

Vijayaparthasarathi Vijayakumar − *Department of Chemistry, School of Advanced Sciences, Vellore Institute of Technology, Vellore 632014 Tamil Nadu, India*; orcid.org/0000-0002-0744-7986; Email: kvpsvijayakumar@gmail.com

Authors

Narayanaswamy Lohitha − *Department of Chemistry, School of Advanced Sciences, Vellore Institute of Technology, Vellore 632014 Tamil Nadu, India*

Peruru Hemanth Kumar − *Department of Chemistry, School of Advanced Sciences, Vellore Institute of Technology, Vellore 632014 Tamil Nadu, India*

Sundaramoorthy Sarveswari − *Department of Chemistry, School of Advanced Sciences, Vellore Institute of Technology, Vellore 632014 Tamil Nadu, India*; orcid.org/0000-0003-2469-0678

Sanket Rathod − *Department of Pharmaceutical Chemistry, Bharati Vidyapeeth College of Pharmacy, Kolhapur 416013 Maharashtra, India*; orcid.org/0000-0002-8037-5974

Somdatta Chaudhari − *Department of Pharmaceutical Chemistry, PES's Modern College of Pharmacy, Pune 411 044 Maharashtra, India*

Yasinalli Tamboli − *King Abdullah International Medical Research Center (KAIMRC), King Saud Bin Abdulaziz University for Health Sciences, Ministry of National Guard-Health Affairs, Riyadh 14811, Saudi Arabia*; orcid.org/0000-0002-5161-0170

Complete contact information is available at: https://pubs.acs.org/10.1021/acsomega.4c00079

Notes

The authors declare no competing financial interest.

■ ACKNOWLEDGMENTS

The authors are thankful to the administration of VIT University, Vellore, India, for providing facilities to carry out research work, SIF-Chemistry for providing the NMR facility, Chemistry Department, VIT for providing the HRMS facility. V.V. is gratefully thanking the VIT management for characterization support and infrastructure through a seed grant (grant no. SG20230086). I.I. and Y.T. are thankful for support (project RC/17/015/R) by King Abdullah International Medical Research Center (KAIMRC).

■ REFERENCES

(1) Clardy, J.; Walsh, C. Lessons from Natural Molecules. *Nature* **2004**, *432* (7019), 829−837.

(2) Soural, M.; Bouillon, I.; Krchňák, V. Combinatorial Libraries of Bis-Heterocyclic Compounds with Skeletal Diversity. *J. Comb. Chem.* **2008**, *10* (6), 923−933.

(3) Murru, S.; Dooley, C. T.; Nefzi, A. Parallel Synthesis of Bis-Oxazole Peptidomimetics. *Tetrahedron Lett.* **2013**, *54* (51), 7062−7064.

(4) Tributino, J. L. M.; Duarte, C. D.; Corrêa, R. S.; Doriguetto, A. C.; Ellena, J.; Romeiro, N. C.; Castro, N. G.; Miranda, A. L. P.;

Barreiro, E. J.; Fraga, C. A. M. Novel 6-Methanesulfonamide-3,4-Methylenedioxyphenyl-N-Acylhydrazones: Orally Effective Anti-Inflammatory Drug Candidates. *Bioorg. Med. Chem.* **2009**, *17* (3), 1125−1131.
(5) Guo, R. Y.; An, Z.-M.; Mo, L.-P.; Wang, R.-Z.; Liu, H.-X.; Wang, S.-X.; Zhang, Z.-H. Meglumine: A Novel and Efficient Catalyst for One-Pot, Three-Component Combinatorial Synthesis of Functionalized 2-Amino-4H-Pyrans. *ACS Comb. Sci.* **2013**, *15* (11), 557−563.
(6) Lyon, M. A.; Lawrence, S.; Williams, D. J.; Jackson, Y. A. Synthesis and Structure Verification of an Analogue of Kuanoniamine A. *J. Chem. Soc., Perkin Trans. 1* **1999**, *4*, 437−442.
(7) Vandekerckhove, S.; Van Herreweghe, S.; Willems, J.; Danneels, B.; Desmet, T.; de Kock, C.; Smith, P. J.; Chibale, K.; D'hooghe, M. Synthesis of Functionalized 3-5-6- and 8-Aminoquinolines via Intermediate (3-Pyrrolin-1-Yl)- and (2-Oxopyrrolidin-1-Yl)-Quinolines and Evaluation of Their Antiplasmodial and Antifungal Activity. *Eur. J. Med. Chem.* **2015**, *92*, 91−102.
(8) Vlahov, R.; Parushev, St.; Vlahov, J.; Nickel, P.; Snatzke, G. Synthesis of Some New Quinoline Derivatives - Potential Antimalarial Drugs. *Pure Appl. Chem.* **1990**, *62* (7), 1303−1306.
(9) Vivekanand, B.; Mahendra Raj, K.; Mruthyunjayaswamy, B. H. Synthesis, characterization, antimicrobial, DNA-cleavage and antioxidant activities of 3-((5-chloro-2-phenyl-1 H -indol-3-ylimino)-methyl)quinoline-2(1 H)-thione and its metal complexes. *J. Mol. Struct.* **2015**, *1079*, 214−224.
(10) Ahmed, N.; Brahmbhatt, K. G.; Sabde, S.; Mitra, D.; Singh, I. P.; Bhutani, K. K. Synthesis and Anti-HIV Activity of Alkylated Quinoline 2,4-Diols. *Bioorg. Med. Chem.* **2010**, *18* (8), 2872−2879.
(11) Pertz, H. H.; Milhahn, H.-C.; Eich, E. Cycloalkanecarboxylic Esters Derived from Lysergol, Dihydrolysergol-I, and Elymoclavine as Partial Agonists and Antagonists at Rat 5-HT2A Receptors: Pharmacological Evidence That the Indolo[4,3-Fg]Quinoline System of the Ergolines Is Responsible for High 5-HT2A Receptor Affinity. *J. Med. Chem.* **1999**, *42* (4), 659−668.
(12) Maguire, M. P.; Sheets, K. R.; McVety, K.; Spada, A. P.; Zilberstein, A. A New Series of PDGF Receptor Tyrosine Kinase Inhibitors: 3-Substituted Quinoline Derivatives. *J. Med. Chem.* **1994**, *37* (14), 2129−2137.
(13) Gemma, S.; Savini, L.; Altarelli, M.; Tripaldi, P.; Chiasserini, L.; Coccone, S. S.; Kumar, V.; Camodeca, C.; Campiani, G.; Novellino, E.; Clarizio, S.; Delogu, G.; Butini, S. Development of Antitubercular Compounds Based on a 4-Quinolylhydrazone Scaffold. Further Structure-Activity Relationship Studies. *Bioorg. Med. Chem.* **2009**, *17* (16), 6063−6072.
(14) Yamakawa, T.; Mitsuyama, J.; Hayashi, K. In Vitro and in Vivo Antibacterial Activity of T-3912, a Novel Non-Fluorinated Topical Quinolone. *J. Antimicrob. Agents* **2002**, *49* (3), 455−465.
(15) Zhi, C.; Long, Z.; Manikowski, A.; Comstock, J.; Xu, W.-C.; Brown, N. C.; Tarantino, P. M.; Holm, K. A.; Dix, E. J.; Wright, G. E.; Barnes, M. H.; Butler, M. M.; Foster, K. A.; LaMarr, W. A.; Bachand, B.; Bethell, R.; Cadilhac, C.; Charron, S.; Lamothe, S.; Motorina, I.; Storer, R. Hybrid Antibacterials. DNA Polymerase-Topoisomerase Inhibitors. *J. Med. Chem.* **2006**, *49* (4), 1455−1465.
(16) Van De Laar, F. A. Alpha-Glucosidase Inhibitors in the Early Treatment of Type 2 Diabetes. *Vasc. Health Risk Manage.* **2008**, *4*, 1189.
(17) Taha, M.; Tariq Javid, M.; Imran, S.; Selvaraj, M.; Chigurupati, S.; Ullah, H.; Rahim, F.; Khan, F.; Islam Mohammad, J.; Mohammed Khan, K. Synthesis and Study of the α-Amylase Inhibitory Potential of Thiadiazole Quinoline Derivatives. *Bioorg. Chem.* **2017**, *74*, 179−186.
(18) Agarwal, P.; Gupta, R. Alpha-Amylase Inhibition Can Treat Diabetes Mellitus. *Res. Rev.: J. Med. Health Sci.* **2016**, *5* (4), 1−8.
(19) Radoi, V.; Lixandru, D.; Mohora, M.; Virgolici, B. Advanced Glycation End Products in Diabetes Mellitus: Mechanism of Action and Focused Treatment. *Proc. Rom. Acad., Ser. B: Chem., Life Sci. Geosci.* **2012**, *1*, 9−19.
(20) Nazir, M.; Abbasi, M. A.; Aziz-ur-Rehman; Siddiqui, S. Z.; Khan, K. M.; Kanwal; Salar, U.; Shahid, M.; Ashraf, M.; Arif Lodhi, M.; Ali Khan, F. New Indole Based Hybrid Oxadiazole Scaffolds with N-Substituted Acetamides: As Potent Anti-Diabetic Agents. *Bioorg. Chem.* **2018**, *81*, 253−263.
(21) Kumar, P. H.; Rambabu, M.; Vijayakumar, V.; Sarveswari, S. Palladium-Mediated Synthesis of 2-([Biphenyl]-4-yloxy) quinolin-3-carbaldehydes through Suzuki-Miyaura Cross-Coupling and Their in Silico Breast Cancer Studies on the 3ERT Protein. *ACS Omega* **2023**, *8* (13), 11806−11812.
(22) Kilbile, J. T.; Tamboli, Y.; Ansari, S. A.; Rathod, S. S.; Choudhari, P. B.; Alkahtani, H.; Sapkal, S. B. Synthesis, Biological Evaluation, and Computational Studies of 6-Fluoro-3-(Piperidin-4-Yl)-1,2-Benzisoxazole Sulfonamide Conjugates. *Polycyclic Aromat. Compd.* **2023**, 1−21.
(23) Bakale, R. D.; Sulakhe, S. M.; Kasare, S. L.; Sathe, B. P.; Rathod, S. S.; Choudhari, P. B.; Madhu Rekha, E.; Sriram, D.; Haval, K. P. Design, Synthesis and Antitubercular Assessment of 1, 2, 3-Triazole Incorporated Thiazolylcarboxylate Derivatives. *Bioorg. Med. Chem. Lett.* **2024**, *97*, 129551.
(24) Rathod, S.; Bhande, D.; Pawar, S.; Gumphalwad, K.; Choudhari, P.; More, H. Identification of Potential Hits against Fungal Lysine Deacetylase Rpd3 via Molecular Docking, Molecular Dynamics Simulation, DFT, In-Silico ADMET and Drug-Likeness Assessment. *Chem. Afr.* **2024**, *7*, 1151−1164.
(25) Choudhari, S.; Patil, S. K.; Rathod, S. Identification of Hits as Anti-Obesity Agents against Human Pancreatic Lipase via Docking, Drug-Likeness, in-Silico ADME(T), Pharmacophore, DFT, Molecular Dynamics, and MM/PB(GB)SA Analysis. *J. Biomol. Struct. Dyn.* **2023**, 1−23.
(26) Rochlani, S.; Bhatia, M.; Rathod, S.; Choudhari, P.; Dhavale, R. Exploration of Limonoids for Their Broad Spectrum Antiviral Potential via DFT, Molecular Docking and Molecular Dynamics Simulation Approach. *Nat. Prod. Res.* **2023**, *38*, 891−896.
(27) Patial, P. K.; Cannoo, D. S. Phytochemical Profile, Antioxidant Potential and DFT Study of Araucaria Columnaris (G. Forst.) Hook. Branch Extracts. *Nat. Prod. Res.* **2021**, *35* (22), 4611−4615.
(28) Amer, M. M. K.; Abdellattif, M. H.; Mouneir, S. M.; Zordok, W. A.; Shehab, W. S. Synthesis, DFT Calculation, Pharmacological Evaluation, and Catalytic Application in the Synthesis of Diverse Pyrano[2,3-c]Pyrazole Derivatives. *Bioorg. Chem.* **2021**, *114*, 105136.
(29) Hunter, A. D. ACD/ChemSketch 1.0 (Freeware); ACD/ChemSketch 2.0 and Its Tautomers, Dictionary, and 3D Plug-Ins; ACD/HNMR 2.0; ACD/CNMR 2.0. *J. Chem. Educ.* **1997**, *74* (8), 905.
(30) Dassault Systèmes. *BIOVIA Discovery Studio Visualizer*; Dassault Systèmes: San Diego, 2020.
(31) Bagal, V. K.; Rathod, S. S.; Mulla, M. M.; Pawar, S. C.; Choudhari, P. B.; Pawar, V. T.; Mahuli, D. V. Exploration of Bioactive Molecules from Tinospora Cordifolia and Actinidia Deliciosa as an Immunity Modulator via Molecular Docking and Molecular Dynamics Simulation Study. *Nat. Prod. Res.* **2023**, *37*, 4053−4057.
(32) O'boyle, N. M.; Banck, M.; James, C. A.; Morley, C.; Vandermeersch, T.; Hutchison, G. R. Open Babel: An Open Chemical Toolbox. *J. Cheminf.* **2011**, *3* (1), 33.
(33) Dallakyan, S.; Olson, A. J. Small-Molecule Library Screening by Docking with PyRx. *Methods Mol. Biol.* **2015**, *1263*, 243−250.
(34) Daina, A.; Michielin, O.; Zoete, V. SwissADME: a free web tool to evaluate pharmacokinetics, drug-likeness and medicinal chemistry friendliness of small molecules. *Sci. Rep.* **2017**, *7*, 42717.
(35) Pires, D. E. V.; Blundell, T. L.; Ascher, D. B. PkCSM: Predicting Small-Molecule Pharmacokinetic and Toxicity Properties Using Graph-Based Signatures. *J. Med. Chem.* **2015**, *58*, 4066−4072.
(36) Rathod, S.; Chavan, P.; Mahuli, D.; Rochlani, S.; Shinde, S.; Pawar, S.; Choudhari, P.; Dhavale, R.; Mudalkar, P.; Tamboli, F. Exploring Biogenic Chalcones as DprE1 Inhibitors for Antitubercular Activity via in Silico Approach. *J. Mol. Model.* **2023**, *29* (4), 113.
(37) Jia, C. Y.; Li, J. Y.; Hao, G. F.; Yang, G. F. A Drug-Likeness Toolbox Facilitates ADMET Study in Drug Discovery. *Drug Discovery Today* **2020**, *25* (1), 248−258.

https://doi.org/10.1021/acsomega.4c00079
ACS Omega 2024, 9, 16384−16399

(38) Lipinski, C. A. Lead- and Drug-like Compounds: The Rule-of-Five Revolution. *Drug Discovery Today: Technol.* **2004**, *1* (4), 337−341.
(39) Leeson, P. D.; Springthorpe, B. The Influence of Drug-like Concepts on Decision-Making in Medicinal Chemistry. *Nat. Rev. Drug Discovery* **2007**, *6* (11), 881−890.
(40) Ya'u Ibrahim, Z.; Uzairu, A.; Shallangwa, G.; Abechi, S. Molecular docking studies, drug-likeness and in-silico ADMET prediction of some novel *β*-Amino alcohol grafted 1,4,5-trisubstituted 1,2,3-triazoles derivatives as elevators of p53 protein levels. *Sci. Afr.* **2020**, *10*, No. e00570.
(41) Swami, P.; Rathod, S.; Choudhari, P.; Patil, D.; Patravale, A.; Nalwar, Y.; Sankpal, S.; Hangirgekar, S. Fe3O4@SiO2@TDI@DES: A Novel Magnetically Separable Catalyst for the Synthesis of Oxindoles. *J. Mol. Struct.* **2023**, *1292*, 136079.
(42) Godfrey, O. C.; Anna, I.; Qader, S. W.; Sampathkumar, G.; Nwoha, T. C.; Runde, M.; Nwokolo, O. A.; Iyam, S. O.; Edo, G. D.; Benjamin, I.; Louis, H. Impact of Polar (DMSO, Ethanol, Water) Solvation on Geometry, Spectroscopy (FT-IR, UV, NMR), Quantum Chemical Parameters, and the Antifungal Activities of Benzothiazole Derivative by Molecular Docking Approach. *Chem. Phys. Impact* **2023**, *7*, 100349.
(43) Bursch, M.; Mewes, J.-M.; Hansen, A.; Grimme, S. Best-Practice DFT Protocols for Basic Molecular Computational Chemistry**. *Angew. Chem., Int. Ed. Engl.* **2022**, *61* (42), No. e202205735.
(44) Jensen, F. Atomic Orbital Basis Sets. *Wiley Interdiscip. Rev.: Comput. Mol. Sci.* **2013**, *3* (3), 273−295.
(45) Mardirossian, N.; Head-Gordon, M. Thirty Years of Density Functional Theory in Computational Chemistry: An Overview and Extensive Assessment of 200 Density Functionals. *Mol. Phys.* **2017**, *115* (19), 2315−2372.
(46) Piela, L. Chasing the Correlation Dragon: Density Functional Theory (DFT). *Ideas Quantum Chem.* **2020**, 191−252.
(47) Tirado-Rives, J.; Jorgensen, W. L. Performance of B3LYP Density Functional Methods for a Large Set of Organic Molecules. *J. Chem. Theory Comput.* **2008**, *4* (2), 297−306.
(48) Neese, F. Software Update: The ORCA Program System—Version 5.0. *Wiley Interdiscip. Rev.: Comput. Mol. Sci.* **2022**, *12* (5), No. e1606.
(49) Snyder, H. D.; Kucukkal, T. G. Computational Chemistry Activities with Avogadro and ORCA. *J. Chem. Educ.* **2021**, *98* (4), 1335−1341.
(50) Puthanveedu, V.; Muraleedharan, K. Phytochemicals as Potential Inhibitors for COVID-19 Revealed by Molecular Docking, Molecular Dynamic Simulation and DFT Studies. *Struct. Chem.* **2022**, *33* (5), 1423−1443.
(51) Elkaeed, E. B.; Yousef, R. G.; Elkady, H.; Gobaara, I. M. M.; Alsfouk, B. A.; Husein, D. Z.; Ibrahim, I. M.; Metwaly, A. M.; Eissa, I. H. Design, Synthesis, Docking, DFT, MD Simulation Studies of a New Nicotinamide-Based Derivative: In Vitro Anticancer and VEGFR-2 Inhibitory Effects. *Molecules* **2022**, *27* (14), 4606.
(52) Berman, H. M.; Westbrook, J.; Feng, Z.; Gilliland, G.; Bhat, T. N.; Weissig, H.; Shindyalov, I. N.; Bourne, P. E. The Protein Data Bank. *Nucleic Acids Res.* **2000**, *28* (1), 235−242.
(53) El-Hachem, N.; Haibe-Kains, B.; Khalil, A.; Kobeissy, F. H.; Nemer, G. AutoDock and AutoDockTools for Protein-Ligand Docking: Beta-Site Amyloid Precursor Protein Cleaving Enzyme 1(BACE1) as a Case Study. In *Methods in Molecular Biology*; Humana Press Inc., 2017; Vol. *1598*, pp 391−403.
(54) Bitencourt-Ferreira, G.; Veit-Acosta, M.; de Azevedo, W. F. Hydrogen Bonds in Protein-Ligand Complexes. *Methods Mol. Biol.* **2019**, *2053*, 93−107.
(55) Sahayarayan, J. J.; Rajan, K. S.; Vidhyavathi, R.; Nachiappan, M.; Prabhu, D.; Alfarraj, S.; Arokiyaraj, S.; Daniel, A. N. In-Silico Protein-Ligand Docking Studies against the Estrogen Protein of Breast Cancer Using Pharmacophore Based Virtual Screening Approaches. *Saudi J. Biol. Sci.* **2021**, *28* (1), 400−407.
(56) Bansode, P.; Pore, D.; Tayade, S.; Patil, S.; Choudhari, P.; Rashinkar, G. Remarkable Anti-Breast Cancer Activity and Molecular Docking Studies of Ferrocene Tethered Pyrimidobenzothiazoles and Pyrimidobenzimidazoles. *Results Chem.* **2023**, *5*, 100758.
(57) Al-Sehemi, A. G.; Pannipara, M.; Parulekar, R. S.; Kilbile, J. T.; Choudhari, P. B.; Shaikh, M. H. In Silico Exploration of Binding Potentials of Anti SARS-CoV-1 Phytochemicals against Main Protease of SARS-CoV-2. *J. Saudi Chem. Soc.* **2022**, *26* (3), 101453.
(58) Basha, G. M.; Parulekar, R. S.; Al-Sehemi, A. G.; Pannipara, M.; Siddaiah, V.; Kumari, S.; Choudhari, P. B.; Tamboli, Y. Design and in Silico Investigation of Novel Maraviroc Analogues as Dual Inhibition of CCR-5/SARS-CoV-2 Mpro. *J. Biomol. Struct. Dyn.* **2022**, *40*, 11095−11110.
(59) Bakale, R. D.; Phatak, P. S.; Rathod, S. S.; Choudhari, P. B.; Rekha, E. M.; Sriram, D.; Kulkarni, R. S.; Haval, K. P. In Vitro and in Silico Exploration of Newly Synthesized Triazolyl-Isonicotinohydrazides as Potent Antitubercular Agents. *J. Biomol. Struct. Dyn.* **2023**, 1−20.
(60) Corso, G.; Jing, B.; Stark, H.; Barzilay, R.; Jaakkola, T. Blind Protein-Ligand Docking with Diffusion-Based Deep Generative Models. *Biophys. J.* **2023**, *122* (3), 143a.
(61) Rathod, S.; Shinde, K.; Porlekar, J.; Choudhari, P.; Dhavale, R.; Mahuli, D.; Tamboli, Y.; Bhatia, M.; Haval, K. P.; Al-Sehemi, A. G.; Pannipara, M. Computational Exploration of Anti-Cancer Potential of Flavonoids against Cyclin-Dependent Kinase 8: An In Silico Molecular Docking and Dynamic Approach. *ACS Omega* **2023**, *8* (1), 391−409.
(62) Shivanika, C.; Deepak Kumar, S.; Ragunathan, V.; Tiwari, P.; Sumitha, A.; Brindha Devi, P. Molecular Docking, Validation, Dynamics Simulations, and Pharmacokinetic Prediction of Natural Compounds against the SARS-CoV-2 Main-Protease. *J. Biomol. Struct. Dyn.* **2022**, *40* (2), 585−611.
(63) Rathod, S.; Dey, S.; Pawar, S.; Dhavale, R.; Choudhari, P.; Rajakumara, E.; Mahuli, D.; Bhagwat, D.; Tamboli, Y.; Sankpal, P.; Mali, S.; More, H. Identification of Potential Biogenic Chalcones against Antibiotic Resistant Efflux Pump (AcrB) via Computational Study. *J. Biomol. Struct. Dyn.* **2023**, 1−19.
(64) Bowers, K. J.; Chow, E.; Xu, H.; Dror, R. O.; Eastwood, M. P.; Gregersen, B. A.; Klepeis, J. L.; Kolossvary, I.; Moraes, M. A.; Sacerdoti, F. D.; Salmon, J. K.; Shan, Y.; Shaw, D. E. Scalable Algorithms for Molecular Dynamics Simulations on Commodity Clusters. *Proceedings of the 2006 ACM/IEEE Conference on Supercomputing, SC'06*, 2006.
(65) Chow, E.; Rendleman, C. A.; Bowers, K. J.; Dror, R. O.; Hughes, D. H.; Gullingsrud, J.; Sacerdoti, F. D.; Shaw, D. E. Desmond Performance on a Cluster of Multicore Processors Hardware and Operating Environment Benchmark Systems and Simulation Parameters. *DE Shaw Research Technical Report DESRES/TR-2008−01*, 2008.
(66) Shivakumar, D.; Williams, J.; Wu, Y.; Damm, W.; Shelley, J.; Sherman, W. Prediction of Absolute Solvation Free Energies Using Molecular Dynamics Free Energy Perturbation and the Opls Force Field. *J. Chem. Theory Comput.* **2010**, *6* (5), 1509−1519.
(67) Jorgensen, W. L.; Chandrasekhar, J.; Madura, J. D.; Impey, R. W.; Klein, M. L. Comparison of Simple Potential Functions for Simulating Liquid Water. *J. Chem. Phys.* **1983**, *79* (2), 926−935.
(68) Bhandari, S. V.; Kuthe, P. V.; Patil, S. M.; Nagras, O. G.; Sarkate, A. P.; Chaudhari, S. Y.; Surve, S. V. Molecular Docking, Pharmacokinetic and Molecular Simulation Analysis of Novel Mono-Carbonyl Curcumin Analogs as L858R/T790M/C797S Mutant EGFR Inhibitors. *Chem. Biodivers* **2023**, *20*, No. e202301081.
(69) Gopinath, P.; Kathiravan, M. K. Docking Studies and Molecular Dynamics Simulation of Triazole Benzene Sulfonamide Derivatives with Human Carbonic Anhydrase IX Inhibition Activity. *RSC Adv.* **2021**, *11* (60), 38079−38093.
(70) Martyna, G. J.; Klein, M. L.; Tuckerman, M. Nosé-Hoover Chains: The Canonical Ensemble via Continuous Dynamics. *J. Chem. Phys.* **1992**, *97* (4), 2635−2643.

https://doi.org/10.1021/acsomega.4c00079
ACS Omega 2024, 9, 16384−16399

(71) Martyna, G. J.; Tobias, D. J.; Klein, M. L. Constant Pressure Molecular Dynamics Algorithms. *J. Chem. Phys.* **1994**, *101* (5), 4177−4189.
(72) Dey, S.; Rathod, S.; Gumphalwad, K.; Yadav, N.; Choudhari, P.; Rajakumara, E.; Dhavale, R.; Mahuli, D. Exploring α, β-unsaturated carbonyl compounds against bacterial efflux pumps *via* computational approach. *J. Biomol. Struct. Dyn.* **2023**, 1−14.
(73) Gaikwad, N. M.; Chaudhari, P. D.; Shaikh, K. S.; Chaudhari, S. Y.; Saleem, R. M.; Algahtani, M.; Altyar, A. E.; Albadrani, G. M.; Kamel, M.; Abdel-Daim, M. M. Albendazole Repurposing on VEGFR-2 for Possible Anticancer Application: In-Silico Analysis. *PLoS One* **2023**, *18* (8), No. e0287198.

https://doi.org/10.1021/acsomega.4c00079
ACS Omega 2024, 9, 16384−16399